eLife

Reviewed Preprint
v1 • June 24, 2025
Not revised

Reviewed Preprint
v2 • July 2, 2026
Revised by authors

Midbrain somatostatin-expressing cells control pain-suppression during defensive states

Nanci Winke[1,2,§], Frank Aby[3,§], Daniel Jercog[1,2,§], Coline Riffault[1,2], Rabia Bouali-Benazzouz[3], Juliette Viellard[1,2,3], Delphine Girard[1,2], Zoé Grivet[3], Marc Landry[3], Laia Castell[4], Emmanuel Valjent[4,5], Stephane Valerio[1,2,*], Pascal Fossat[3,*], Cyril Herry[1,2,*]

[1]Univ. Bordeaux, Neurocentre Magendie, U1215, Bordeaux, France • [2]INSERM, Neurocentre Magendie, U1215, Bordeaux, France • [3]Univ. Bordeaux, CNRS, Institute for Neurodegenerative Diseases, IMN, UMR 5293, Bordeaux, France • [4]Université de Montpellier, Institut de génomique fonctionnelle (IGF), CNRS, Inserm, Montpellier, France • [5]INM, Univ. Montpellier, Inserm, Montpellier, France

For correspondence:
nanci.winke@inserm.fr
cyril.herry@inserm.fr

[§] shared authorship

[*] shared seniority

Competing interests: No competing interests declared

Funding: See page 30

Reviewing editor: Michael A McDannald, Boston College, United States

eLife Assessment

This **important** study shows that long-range somatostatin-expressing neurons in the ventrolateral periaqueductal grey that project to the rostral ventromedial medulla selectively suppress pain responses during conditioned fear. The evidence supporting these conclusions is **exceptional**, with methods spanning a novel cued fear-conditioned analgesia paradigm, cell-type-specific optogenetic activation and inhibition, anatomical circuit tracing, and in vivo spinal cord electrophysiology. These results will be of broad interest to systems and behavioral neuroscientists studying fear, pain, and descending pain-control circuitry.

https://doi.org/10.7554/eLife.106826.2.sa4

Abstract

In threatening situations, animals exhibit a broad range of behavioral and autonomic responses. As such, a crucial adaptive response is the inhibition of pain, which facilitates relevant defensive behaviors that promote survival. Whereas the structures and mechanisms involved in fear and pain behaviors are well documented, little is known about the precise neuronal mechanisms mediating the emotional regulation of endogenous pain-suppression. Here, we used a combination of behavioral, anatomical, optogenetic, and electrophysiological approaches to investigate, in male mice, the role of somatostatin-expressing cells in the ventrolateral periaqueductal gray matter (SST^+ vlPAG cells) in the control of analgesia induced during defensive states. Our data indicate that optogenetic inhibition of SST^+ vlPAG cells promotes analgesia irrespective of animal defensive state. In contrast, optogenetic activation of long-range SST^+ vlPAG cells that project to the rostral ventromedial medulla (RVM) abolishes the analgesia mediated by fear behavior. Together, these results identify a novel circuit mechanism composed of long-range SST^+ vlPAG cells projecting to the RVM that regulate analgesia elicited during defensive states.

Introduction

During threatening situations, the inhibition of pain is an essential adaptive response that can be crucial to promote self-preservation[1–4]. The inhibition of pain responses to a stimulus that would typically elicit pain is defined as analgesia[5]. In addition, previous studies have described that a fearful event can reduce pain sensitivity, a phenomenon referred to as fear-conditioned analgesia (FCA)[6]. In particular, pharmacological inactivation of the basolateral amygdala abolishes this fear-modulated analgesia and is associated with increased immediate-early gene c-Fos expression in

the central amygdala and periaqueductal gray matter (PAG)[7]. The PAG is a midbrain structure that receives many cortical and subcortical inputs from brain structures involved in fear processing[8–11], projecting to the spinal cord primarily through a brainstem relay in the rostral ventromedial medulla (RVM)[12], a key structure involved in nociceptive transmission[13,14]. Indeed, the ventrolateral part of the PAG (vlPAG) is crucial for the descending control of pain[13,15] in the dorsal horn of the spinal cord (DH)[12], and several reports indicate that electrical stimulation of the vlPAG selectively inhibits responses to noxious stimuli in a variety of pain test conditions[12]. Moreover, analgesia induced upon vlPAG stimulation is opioid-dependent[16–18] and involves direct descending projections to the RVM and the DH[19–22]. Furthermore, previous research indicates that activation of the vlPAG induces analgesia through the recruitment of local GABAergic cells[23], which is consistent with our understanding of the role of the GABAergic system in the descending control of pain[24,25]. Thus, the vlPAG is ideally positioned to mediate the emotional regulation of pain behavior, yet the underlying neuronal circuits and mechanisms are largely unknown. Here, we investigated the precise neural circuits within the vlPAG that mediate the suppression of pain behavior during threatening situations. We developed a unique behavioral paradigm where a cued-elicited defensive state promotes changes in pain sensitivity. Combining behavioral, anatomical, optogenetic, and electrophysiological approaches, we identified a novel midbrain to brainstem circuit mechanism composed of somatostatin positive (SST^+) vlPAG cells projecting to the RVM that is critically involved in the suppression of pain behavior during conditioned fear states.

Results

Cued-fear conditioning elicits analgesia

To evaluate the contribution of specific vlPAG cell populations to the fear modulation of pain behavior, we developed a novel cued fear-conditioned analgesia (CFCA) paradigm, consisting of a pain sensitivity assay during the presentation of threat-predicting cues (Figure 1a). In this paradigm, an initially neutral stimulus (the conditioned stimulus, CS^+) becomes associated with a footshock (the unconditioned stimulus, US), whereas another neutral stimulus serves as a control (CS^-). After conditioning, re-exposure to the CS^+ elicited freezing behavior, a behavioral readout of associative learned fear[26] (Figure 1b and Supplementary Figure 1a). Following the fear retrieval session, male mice were submitted to the pain sensitivity assay. Mice were placed on a Hot-Plate (HP) apparatus in which the floor plate temperature progressively increases while either CS^- or CS^+ were concomitantly presented. Plate temperature increased, and CSs were continuously played until mice displayed a nociceptive (NC) response reflecting pain behavior (Figure 1c), defined by either jumping or hindpaw licking (Figure 1d). The detection of a NC response terminated the test session (**see Methods**).

We observed a significant delay in the NC response performance for CS^+ compared to CS^- presentations, reflecting that pain-suppression was selectively promoted by the threat-predicting CS (Figure 1e and Supplementary Figure 1b). This increased NC latency during CS^+ presentation could alternatively be explained by a competition between freezing and pain-related responses. However, freezing probability at the time of the NC response for CS^+ was remarkably low and comparable to CS^- levels, suggesting that CS^+ increased NC response latency was not due to competing freezing responses (Figure 1f, **see Methods**). Instead, these results suggest that fear induced by CS^+ presentations drives the increase in NC latency. Importantly, such states induced by our CFCA paradigm reflected fear associative processes (Supplementary Figure 2). To demonstrate a causal link between cued-fear and analgesia, mice were submitted to an extinction procedure to devalue the CS^+-US contingency and abolish the negative emotional state during CS^+ presentations (Figure 1g). Under these conditions, CS^+ presentation after extinction had no effects on NC response latency (Figure 1h). Furthermore, the absence of auditory cues, or the presence of auditory cues not associated with a threat, led to NC response latencies comparable to those observed during CS^- presentations (Figure 1i). Finally, previous studies indicate that fear can lead to vasoconstriction, which could result in a redirection of the blood flow to the skeletal musculature, decreasing the temperature in the extremities of the body[27]. However, monitoring

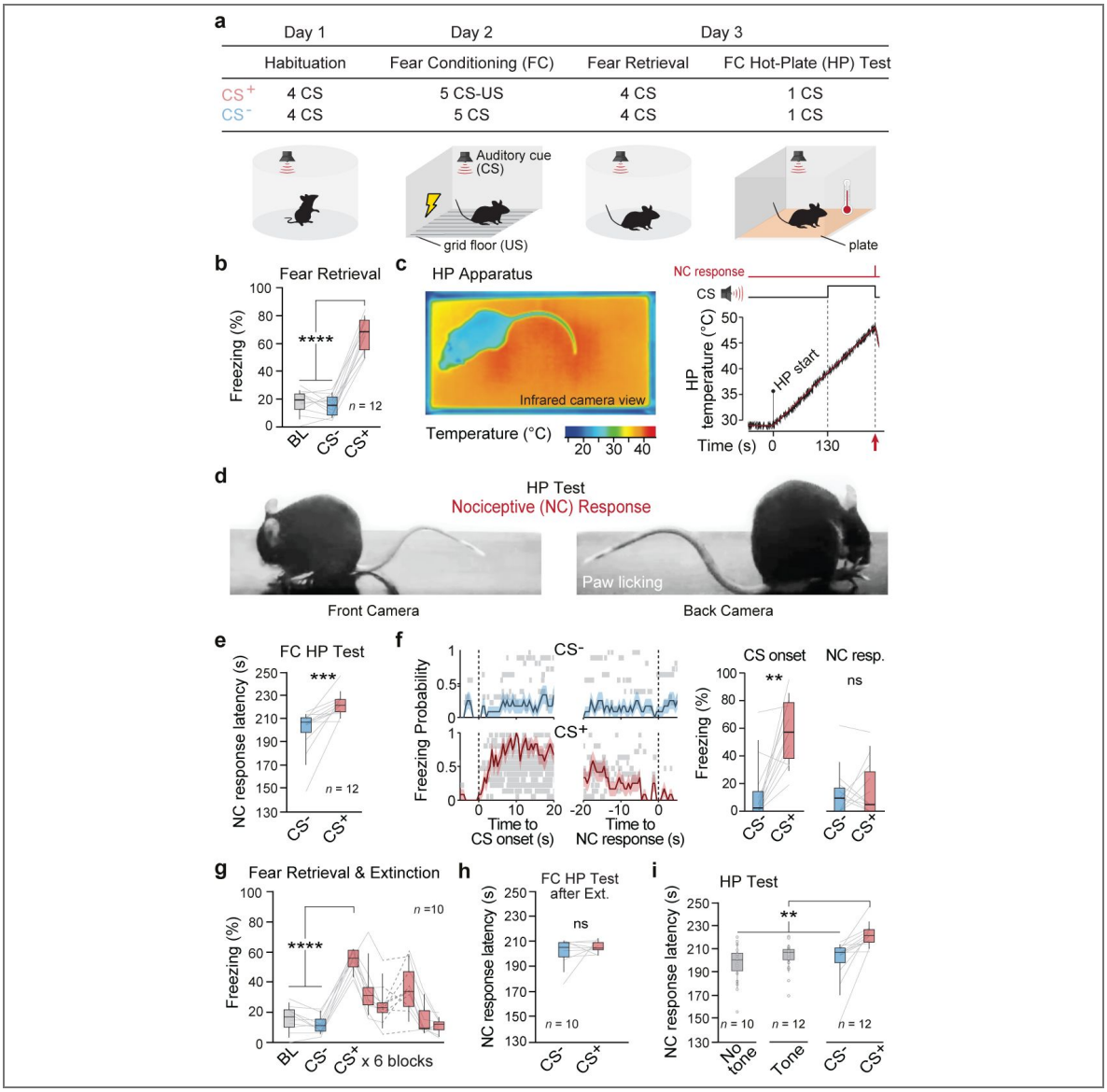

Figure 1. Fear modulation of pain behavior.

a. Schematic of the setup and the CFCA paradigm. The paradigm consists of a discriminative auditory fear conditioning test followed by a pain sensitivity assay (for details, see Methods). **b.** Average freezing values for CS^+ were higher than CS^- or baseline (BL) periods during retrieval (****, $P < 0.0001$, one-way RM ANOVA, n = 12 mice). **c.** Example of the infrared digital thermographic camera view of a mouse during the FC HP test. After 1 min of context acclimatization, the plate temperature steadily increases at 6 °C per min (HP start). CSs started 130 s after the HP start and continued until mice displayed an NC response (licking the hindpaw or jumping). **d.** Example of assessed hindpaw licking NC response. **e.** Latency of NC response on the FC HP test increased during CS^+ compared to CS^- (***, $P = 0.0005$, Wilcoxon matched-pairs signed rank test, n = 12 mice). **f. Left**: dynamics of freezing probability at CS onset and NC response for both CS^- and CS^+ (freezing periods for each individual mouse are displayed by rows in grey; error bars display S.E.M; bin size = 0.5 s). **Right**: average freezing values during 10 s after CS onset and before NC response for CS^+ were higher than CS^- only at CS onset (***, $P_{onset} = 0.0015$, paired t-test, n = 12 mice). **g.** Mean freezing values during fear extinction, 24 CS^+ were presented across two separate extinction sessions (joined by dashed lines). Mice acquired the CS^+-US association (1st CS^+ block vs. BL/CS^- ****, $P < 0.0001$, Friedman test, n = 10 mice), followed by a rapid extinction (5th & 6th block of CS^+ vs BL/CS- ns, $P > 0.05$, one-way RM ANOVA). **h.** After extinction, there was no difference in the NC response latency for both CSs (ns, $P > 0.05$, paired t-test n = 10 mice). **i.** Average NC response latencies for the different HP tests. *No tone* - mice submitted to the HP test without conditioning nor tone presentation. *Tone* - mice submitted to the HP test paired with unconditioned tone presentation. *CS^-/CS^+* - mice were submitted to the CFCA protocol. (No tone/Tone/CS^- vs. CS^+ **, $P < 0.0001$, Krustal-Wallis test). For exact P values and test statistics on this and all subsequent figures, see Supplementary Table 1.

the back and tail temperatures of mice submitted to the HP test did not reveal any differences between the CSs presentations, suggesting that the increased latency was not due to fear-induced vasoconstriction (Supplementary Figure 1c-e). Overall, our results indicate that the presence of a conditioned threat-predicting cue can selectively promote analgesia.

Photostimulation of SST$^+$ vlPAG cells alters pain and fear behavior

To identify the cell types in the vlPAG mediating the analgesic effect in the CFCA task, we focused on GABAergic interneurons, whose activity is suggested to be inhibited during analgesia through μ-opioid receptor-dependent mechanisms[12,25]. Using single-molecule fluorescent in situ hybridization (smFISH, **see Methods**), we confirmed that the majority of vlPAG SST mRNAs were expressed in inhibitory neurons (Supplementary Figure 3). As such, since somatostatin-expressing interneurons (SST) are the most abundant interneuron class in the vlPAG[28], we focused on this cell population. Thus, to evaluate the contribution of SST$^+$ vlPAG cells in CFCA, SST-Cre mice were injected in the vlPAG with a Cre-dependent AAV expressing the Channelrhodopsin (ChR2), Archaerhodopsin (ArchT), or GFP while optic fibers were bilaterally implanted targeting this area (Figure 2a, Supplementary Figure 11). Next, mice were submitted to the CFCA task while photostimulating SST$^+$ cells in the vlPAG (Figure 2b; **see Methods**). After fear retrieval (Figure 2c, e; Supplementary Figure 4a-d), the optogenetic activation of SST$^+$ vlPAG cells during the HP test had no effect on CS$^-$ presentation, whereas the same manipulation performed during CS$^+$ blocked the increase in NC response latency compared to GFP controls (Figure 2d and Supplementary Figure 5a). In contrast, optogenetic inhibition of SST$^+$ vlPAG cells increased NC response latency for both CS$^-$ and CS$^+$ conditions compared to GFP controls (Figure 2f and Supplementary Figure 5b). Importantly, these changes in NC response latencies were not due to motor or aversive effects of the optogenetic manipulations, since photoactivation of SST$^+$ vlPAG cells did not induce changes in distance traveled in an open field nor place aversion in a real-time place preference test (Supplementary Figure 5c-f). In addition, we did not observe changes in fear learning or expression when the footshock was replaced or paired with photoactivation of the SST$^+$ vlPAG cells during the fear conditioning procedure (Supplementary Figure 6).

Altogether, these experiments confirmed that SST$^+$ vlPAG activation did not promote pain responses and instead suggested that the SST$^+$ vlPAG cells are key elements of an endogenous pain-suppression circuit. Additionally, the optogenetic effect observed during CFCA was not due to alteration of somatostatin levels in our homozygous SST-Cre mice[29], as we observed the same effect in heterozygous SST-Cre mice (Supplementary Figure 7a-d). Finally, in contrast with STT$^+$ vlPAG cells, the optogenetic inhibition of another important class of vlPAG inhibitory cells expressing the vasoactive intestinal peptide (VIP$^+$) did not change the NC response latencies during CS$^-$ or CS$^+$ presentations (Supplementary Figure 7e-h, Supplementary Figure 10).

Because our CFCA paradigm is dependent on fear associative processes (Figure 1 and Supplementary Figure 1-2), it is possible that the optogenetic manipulation of SST$^+$ vlPAG cells may have altered the expression of fear behavior. To control for this possibility, we optogenetically activated or inhibited SST$^+$ vlPAG cells during a fear retrieval session following auditory fear conditioning (Figure 3a, b). Our data indicate that whereas optogenetic inhibition of SST$^+$ vlPAG cells had no effect on freezing behavior relative to GFP controls, their optogenetic activation reduced freezing levels (Figure 3c, d). Altogether, our data show that the local SST$^+$ vlPAG network can modulate both fear expression and the analgesia promoted during defensive states.

Photostimulation of SST$^+$ vlPAG cells regulates spinal cord nociceptive transmission

Consistent with our observations, previous studies found that the vlPAG is involved in fear-conditioned analgesia[7]. It is conceivable that the SST$^+$ vlPAG cells are indeed part of a circuit involved in the fear regulation of endogenous pain-suppression. To evaluate the effect of the manipulation of SST$^+$ vlPAG cells on analgesia independently of the expression of fear behavior, we evaluated the impact of SST$^+$ vlPAG cells manipulation on the control of nociceptive

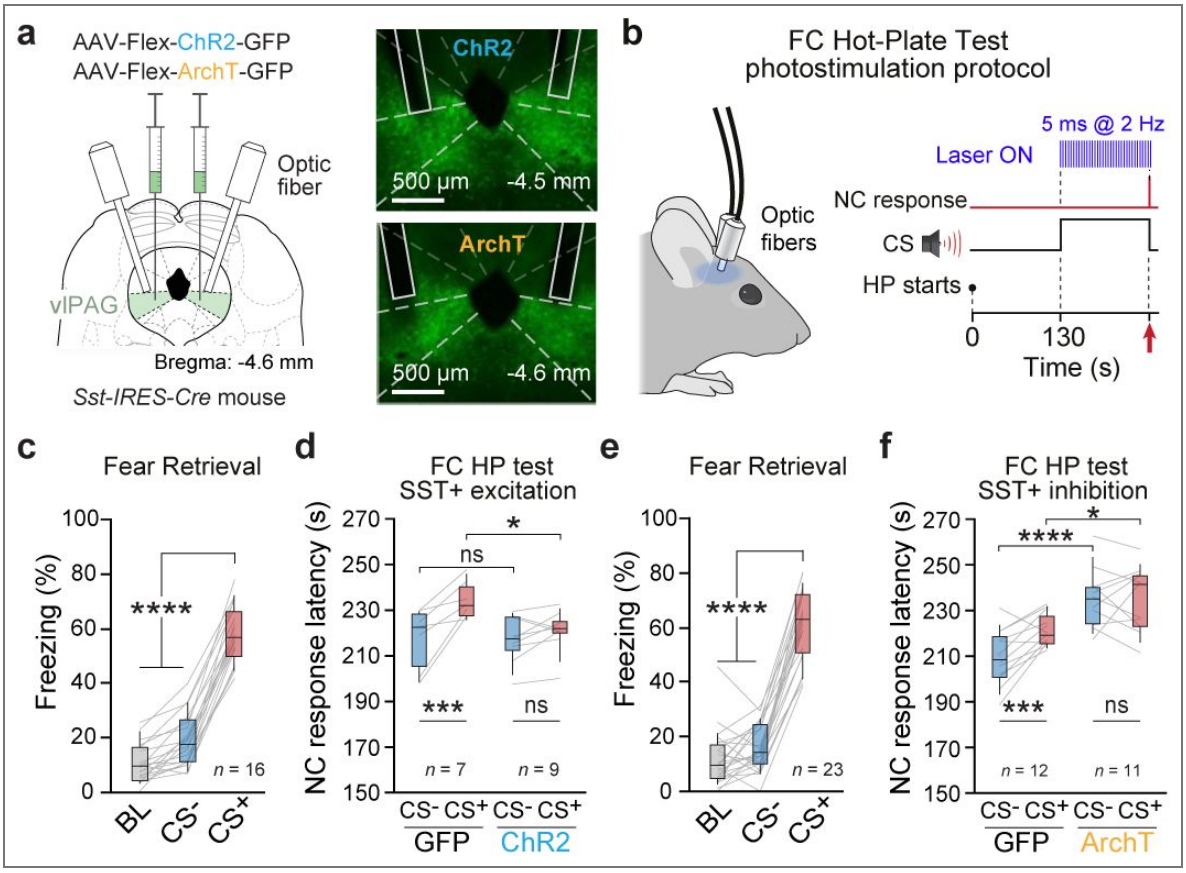

Figure 2. SST$^+$ cells in vlPAG mediate the fear modulation of pain behavior.

a. Sst-IRES-Cre mice were bilaterally injected with viruses that expressed ChR2 (right, upper), ArchT (right, bottom), or GFP (control) in SST$^+$ vlPAG cells. **b**. Schematics of the stimulation protocol used for photoactivation of the SST$^+$ vlPAG cells: blue light delivered at 2 Hz with 5 ms pulse duration during CSs presentation until NC response. For photoinhibition experiments, green light was delivered continuously. **c, e.** Average freezing values during retrieval for ChR2- (**c**) and ArchT-infected mice (**e**) and their respective GFP controls. The opsin and respective control groups were pooled together because no difference was found in the conditioning level (see Supplementary Figure 4). Average freezing values during CS$^+$ were higher than CS$^-$ or baseline (BL) periods (****, P < 0.001, one-way RM ANOVA, (**c**) n = 16 mice and (**e**) n = 23 mice). **d.** Photoactivation of SST$^+$ vlPAG cells abolished the analgesic effect induced by fear (*, P = 0.0112, opsin x CS - two-way RM ANOVA, n = 7 GFP, n = 9 ChR2). The NC response latency for the CS$^+$ was significantly different between the ChR2 and GFP groups (*, P = 0.0344, Bonferroni post-hoc test). For the ChR2 group, the NC response latency during CS$^+$ was equivalent to the CS$^-$ (ns, P = 0.3876, Bonferroni post-hoc test). On the contrary, NC response latency between the CSs differed in the GFP group (***, P = 0.0003, Bonferroni post-hoc test). **f.** Photoinhibition of SST$^+$ vlPAG cells increased the analgesic effect for the ArchT group when compared to the GFP (*, P = 0.0037, opsin x CS - two-way RM ANOVA, n = 12 GFP, n = 11 ArchT). The NC response latency for the CS$^-$and CS$^+$ was significantly different between the ArchT and GFP group (CS$^-$: ****, P < 0.0001, Bonferroni post-hoc test; CS$^+$: *, P = 0.0265, Bonferroni post-hoc test). For the GFP group, the latency of NC response was higher for the CS$^+$ trials when compared to the CS$^-$ trials (***, P = 0.0003, Bonferroni post-hoc test), yet this was not the case for the ArchT group (ns, P > 0.999, Bonferroni post-hoc test).

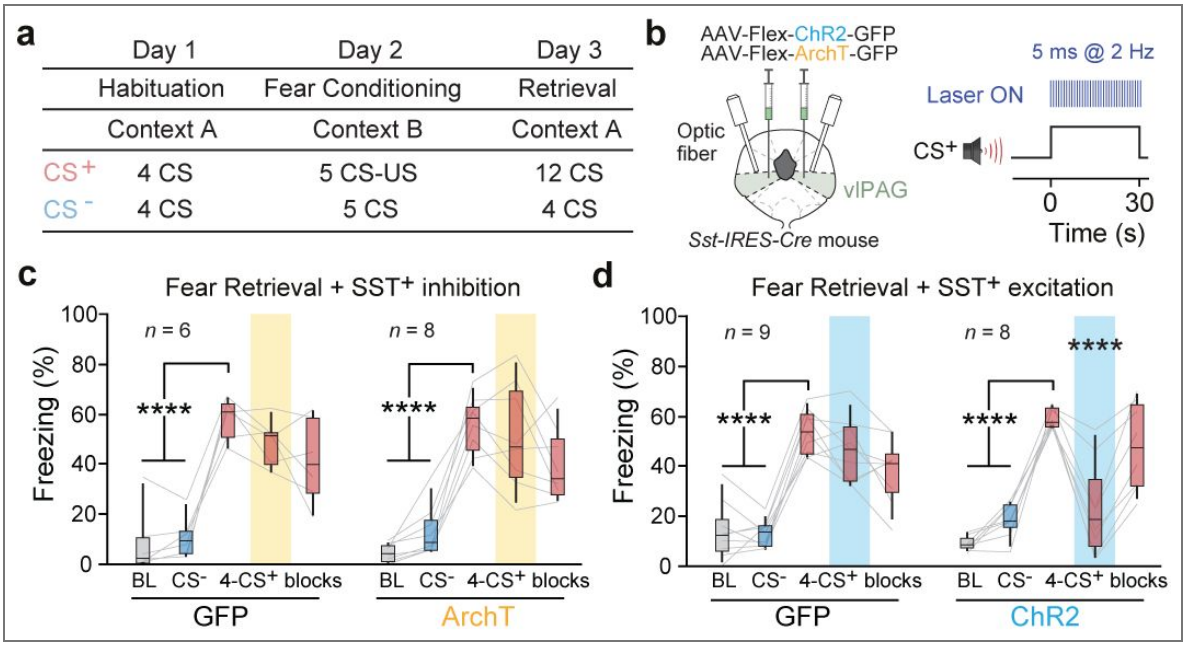

Figure 3. Activation of SST$^+$ vlPAG cells reduced fear expression

a. Protocol for optogenetic manipulation during fear retrieval. Days 1 and 2 were done as described previously for the CFCA paradigm. During retrieval, there were 12 CS$^+$ presentations divided into three blocks. **b.** The stimulation protocol used to photoactivate the SST$^+$ vlPAG cells. The optogenetic manipulation was performed during the 2nd block of the CS$^+$ presentation (analogously to CFCA manipulations, Figure 2b). **c.** Light inhibition of SST$^+$ vlPAG cells did not modulate freezing levels (ArchT ns, P = 0.9396, opsin x CS two-way RM ANOVA, n = 6, GFP, n = 8). **d.** Photoactivation of the SST$^+$ vlPAG cells had no effect on the GFP group, but it transiently decreased the freezing levels for the ChR2 group (***, P < 0.0001, opsin x CS two-way RM ANOVA, n = 9 GFP, n = 8 ChR2).

transmission directly at the level of the spinal cord DH. Therefore, we performed extracellular local field potential and single-unit recordings in the spinal cord DH during optogenetic stimulation of SST$^+$ vlPAG cells in anesthetized mice (Figure 4a). Nociceptive stimulation induces early and late neuronal responses at the level of the spinal cord DH[30] (A- comprising non-nociceptive Aβ and nociceptive A8 and C- fiber mediated, respectively; Figure 4a). While optogenetic activation of SST$^+$ vlPAG cells during suprathreshold electrical stimulation of the paw increased the magnitude of late nociceptive field potentials, the optogenetic inhibition reduced it (Figure 4b, c). To determine whether this effect was specific to the nociceptive network, we recorded wide dynamic range (WDR) cells in the DH, which receive both tactile (Aβ) and nociceptive (Aδ and C) information[30]. We observed that photoactivation of SST$^+$ vlPAG cells increases both fast nociceptive (A8-fiber) and slow nociceptive (C-fiber) responses without affecting non-nociceptive (Aβ-fiber) responses (Figure 4d). Moreover, optogenetic inhibition of SST$^+$ vlPAG cells specifically inhibited nociceptive responses, whereas non-nociceptive responses (Aβ-fiber) remained unaffected (Figure 4e). In addition, we performed subliminal electrical stimulations that did not elicit nociceptive neuronal responses. In this condition, we observed that removing analgesia by activating SST$^+$ vlPAG cells elicited WDR responses at latencies corresponding to nociceptive A8- and C-fibers (Figure 4f). Finally, the optogenetic activation of SST$^+$ vlPAG cells had no effect on purely tactile fast latency spinal neurons (Supplementary Figure 8). Consistent with our optogenetic manipulations during the CFCA task (Figure 2), these data suggest that, under analgesia promoted by isoflurane, activation and inhibition of SST$^+$ vlPAG cells increased and decreased nociceptive transmission, respectively, by specifically promoting pronociceptive and antinociceptive responses in the spinal cord DH.

SST$^+$ vlPAG-RVM-spinal cord pathway activation abolishes analgesia induced during defensive states

We next evaluated whether SST$^+$ vlPAG cells mediate their analgesia modulation by contacting WDR cells directly in the spinal cord or through the rostro ventromedial medulla (RVM), a structure known to receive direct projections from vlPAG and mediate pain modulation[19,20] (Figure 5a). Anatomical tracing revealed large labeling of SST$^+$ fibers in RVM (Figure 5b) and only sparse labeling within the spinal cord (SC; data not shown). By combining fluorogold retrolabeling from the SC and GFP anterograde labeling from SST$^+$ vlPAG cells (Figure 5c), we observed RVM cells projecting to the DH with close apposition of SST$^+$ putative boutons (Figure 5d), suggesting that SST$^+$ vlPAG cells project to the RVM and contact DH-projecting RVM cells. Optogenetic activation of SST descending fibers above the SC has no effect on WDR neural activity upon paw electrical stimulation, suggesting that SST$^+$ vlPAG long-range projections to SC did not play a major role in endogenous pain-suppression (Figure 5e). In contrast, photoactivation of SST$^+$ vlPAG inputs to the RVM increased both nociceptive (A8 and C-fiber) responses (Figure 5f, Supplementary Figure 9). Altogether, these data revealed that the SST$^+$ vlPAG-RVM-DH pathway mediates endogenous pain-suppression.

We next addressed whether the SST$^+$ vlPAG-RVM-DH pathway was specific to mediating endogenous pain-suppression induced by defensive states. Thus, SST-Cre mice were injected in the vlPAG with a Cre-dependent AAV expressing the ChR2 or GFP, and a single optic fiber was implanted above the RVM (Figure 6a). While photoactivation of the SST$^+$ vlPAG-RVM pathway promoted nociception (Figure 5f), it did not impact fear expression as freezing levels remained unchanged (Figure 6b). Consistently, activation of the SST$^+$ vlPAG-RVM pathway during CFCA had no impact on CS$^-$ presentation, whereas the same manipulation performed during CS$^+$ blocked the increase in NC response latency compared to GFP controls (Figure 6c, d). Overall, these data suggest the existence of two populations of SST$^+$ vlPAG cells mediating fear expression and analgesia induced by defensive states. (Figure 6e). Altogether, our results indicate that the SST$^+$ vlPAG-RVM-DH pathway is critically involved in the analgesia induced during defensive states.

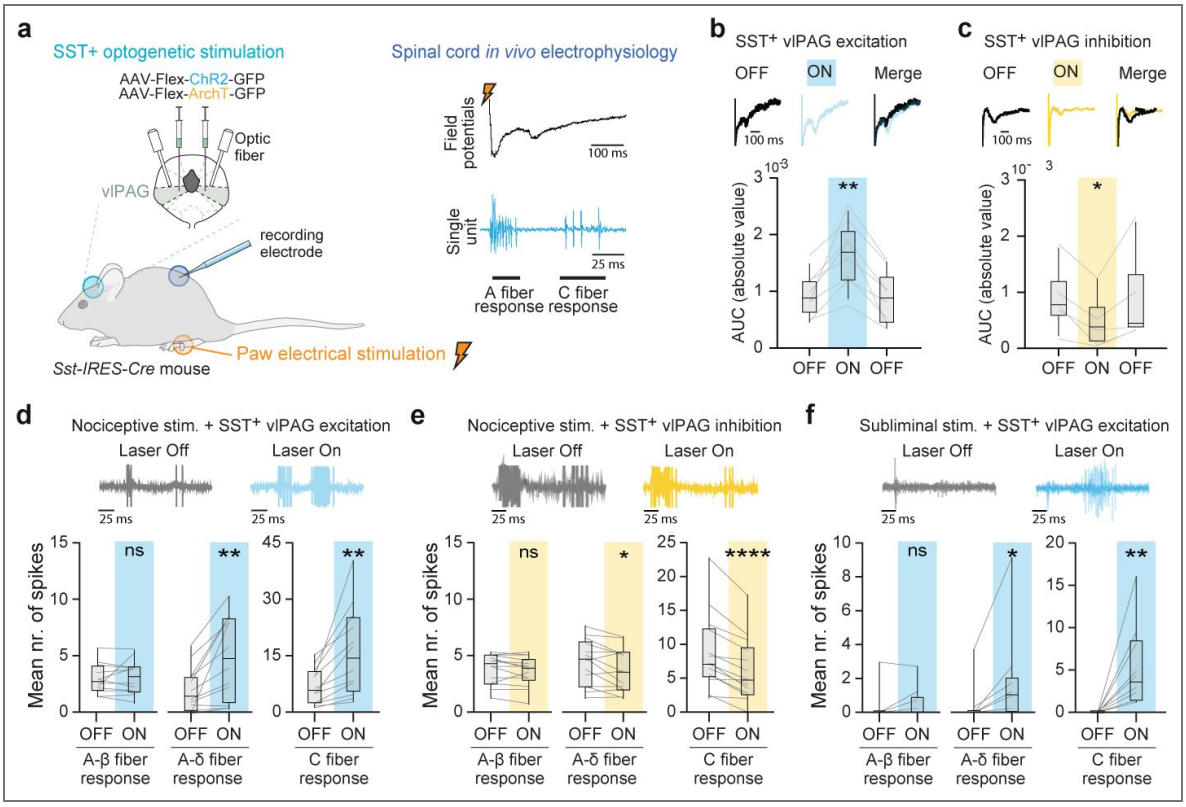

Figure 4. Manipulation of SST$^+$ vlPAG cells alters spinal cord-related pain signals.

a. Schematics of *in vivo* anesthetized experiments. Extracellular local field potential and single-unit recordings in the spinal cord DH were performed during optogenetic stimulation of SST$^+$ vlPAG cells with concomitant noxious electrical paw stimulation**. b.** Example of average nociceptive field potentials in the lumbar SC before (OFF), during (ON), and after (OFF) photoactivation of SST$^+$ vlPAG cells (top). Photoactivation induces a significant increase in the nociceptive fields (bottom; **, P = 0.0001, one-way RM ANOVA, n = 8 mice). **c.** Analogous to panel b, but for photoinhibition of SST$^+$ vlPAG cells. Photoinhibition induces a significant decrease in the nociceptive fields (bottom; *, P = 0.0275, one-way RM ANOVA, n = 5 mice). **d.** Example of WDR single-unit activity before and during photoactivation of SST$^+$ vlPAG cells (**top**). Photoactivation of SST$^+$ vlPAG cells induces a significant and global increase in WDR response to both Aδ- and C-mediated nociceptive fibers (**bottom**; **, $P_{A\delta\ fiber}$ = 0.0022, paired t-test, n = 11 cells; **, $P_{C\ fiber}$ < 0.0033, paired t-test, n = 11 cells). **e.** Analogous to panel d, but for photoinhibition of SST$^+$ vlPAG cells. Photoinhibition induces a significant and specific inhibition of WDR response to Aδ- and C-fibers (**bottom**; *, $P_{A\delta\ fiber}$ = 0.0241, ****, $P_{C\ fiber}$ < 0.0001, n = 14 cells, Wilcoxon matched-pairs signed rank test). **f.** Example traces of single-unit recordings of WDR cells with subthreshold electrical stimulation accompanied by photoactivation of SST$^+$ vlPAG cells (**top**). The photoactivation of SST$^+$ vlPAG cells elicits WDR response to A- and C- mediated peripheral fibers (**bottom**; *, $P_{A\delta\ fiber}$ = 0.0156, n = 10 cells; **, $P_{C\ fiber}$ = 0.0020, n = 10 cells, Wilcoxon matched-pairs signed rank test).

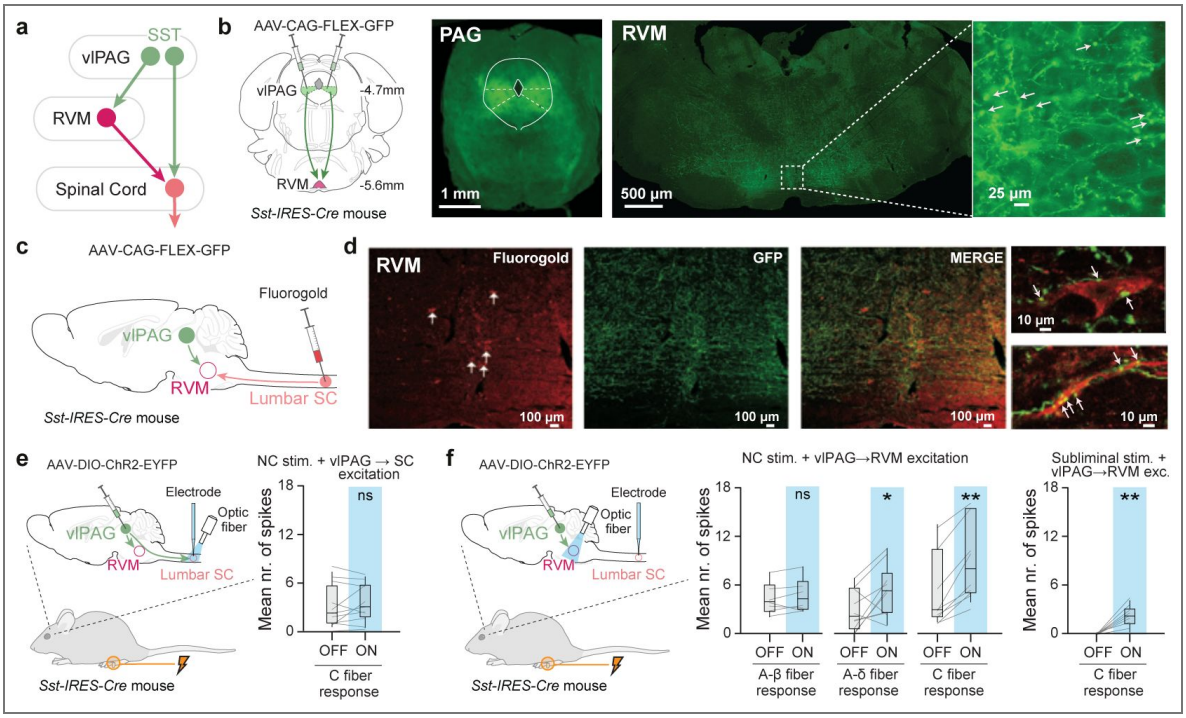

Figure 5. SST$^+$ vlPAG-RVM-DH pathway activation removes analgesia.

a. Schematics of possible SST$^+$ vlPAG circuits mediating analgesia by long-range projections directly to the SC or, alternatively, by projecting to the SC via the rostral ventromedial medulla (RVM). **b.** Sst-IRES-Cre mice were injected with an anterograde AAV Cre-dependent GFP virus in the vlPAG (left). Example of SST fibers labeling at the level of the RVM (middle). Higher magnification (right) reveals putative axonic buttons in the RVM (examples indicated by white arrows). **c.** Sst-IRES-Cre mice were injected concomitantly with anterograde AAV Cre-dependent GFP virus in the vlPAG and retrograde fluorogold in the lumbar DH of the SC. **d.** Fluorogold positive cells (red) cross SST$^+$ vlPAG fibers in the RVM (green). Higher magnification (**right**) shows close contacts between the putative SST$^+$ button and fluorogold$^+$ cells or fibers (white arrows). **e.** Sst-IRES-Cre mice were injected in the vlPAG with AAV Cre-dependent ChR2 virus and an optic fiber placed above the lumbar SC. Single-unit recordings of WDR cells while photoactivation of the SST$^+$ vlPAG SC fibers and electrically stimulating the paw in anesthetized mice (**left**). Photoactivation of vlPAG projections to SC did not affect nociceptive transmission (**right**; ns, P = 0.3683, paired t-test, n = 11 cells). **f.** Same experimental design as in panel e, except that the optic fiber was placed above the RVM (left). Photoactivation of SST$^+$ vlPAG inputs to the RVM induces a significant increase in WDR response to both Aδ- and C-mediated nociceptive fiber stimulation (**middle**; *, $P_{A\delta\ fiber}$ = 0.0346, Paired t-test, n = 10 cells; **, $P_{C\ fiber}$ = 0.0020, Wilcoxon matched-pairs signed rank test, n = 10 cells). Removal of analgesia by activation of SST$^+$ vlPAG-RVM induces a significant increase in WDR response to C-fiber responses (right; **, P = 0.0078, Wilcoxon matched-pairs signed rank test, n = 9 cells).

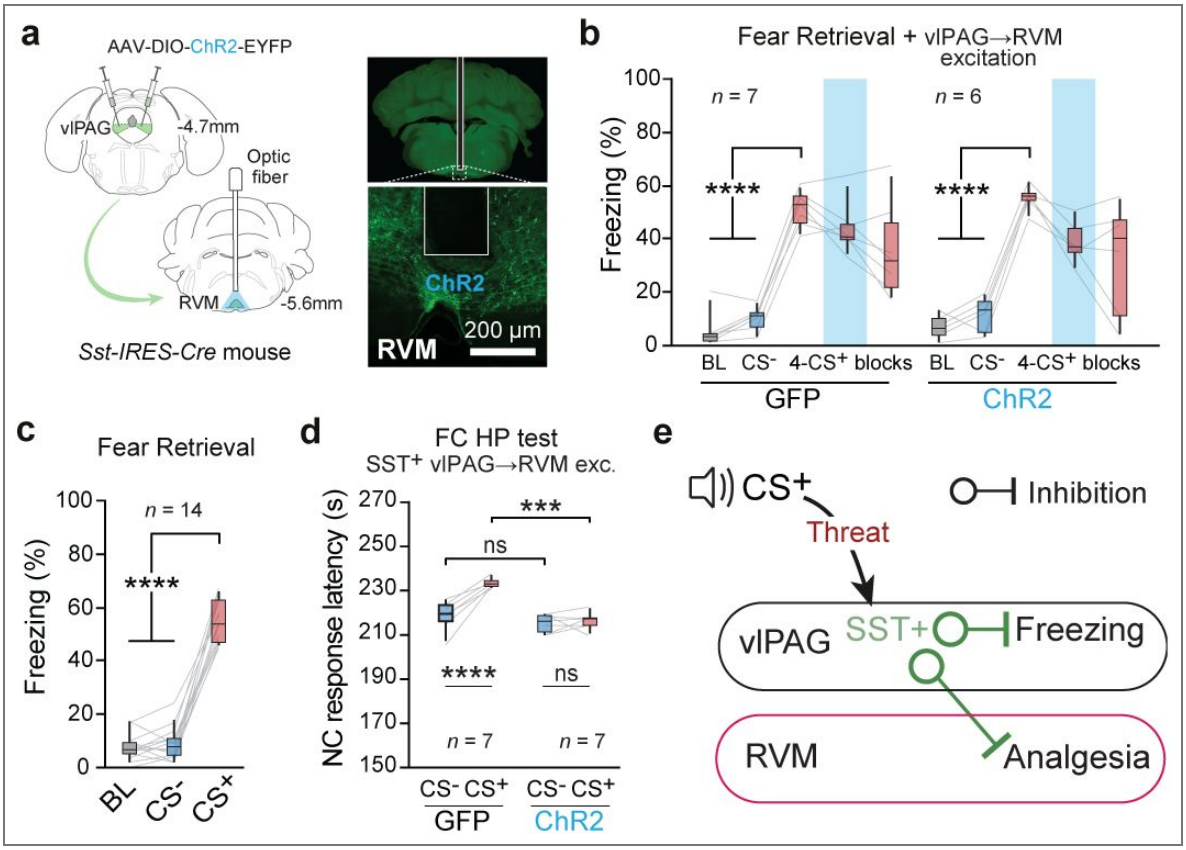

Figure 6. **SST$^+$ vlPAG-RVM-SC pathway activation abolishes analgesia induced by CFCA.**

a. Sst-IRES-Cre mice were bilaterally injected with an AAV expressing ChR2 or GFP in the vlPAG, and optic fibers were implanted above the RVM (left). Representative example of SST$^+$ vlPAG terminals in the RVM (right). **b.** Photoactivation of SST$^+$ vlPAG-RVM pathway did not modulate freezing levels (ns, P = 0.6443, opsin x CS two-way RM ANOVA; CS$^+$ 2nd block, GFP vs. ChR2 ns, P > 0.9999, Bonferroni post-hoc test, n = 7 GFP, n = 6 ChR2). **c.** Average freezing values during retrieval for pooled ChR2 and GFP-infected mice (groups were pooled together since no difference was found in the conditioning level). Average freezing values during CS$^+$ were higher than CS$^-$ or baseline (BL) periods (****, P < 0.0001, one-way RM ANOVA, n = 14 mice). **d.** Photoactivation of SST$^+$ vlPAG-RVM pathway abolished the analgesic effect modulated by fear (**, P = 0.0063, opsin x CS - two-way RM ANOVA, n = 7 GFP, n = 7 ChR2). For the ChR2 group, the NC response latency during CS$^+$ was equivalent to the CS$^-$ (ns, P > 0.9999, Bonferroni post-hoc test). On the contrary, the NC response latency between the CSs differed in the GFP group (****, P < 0.0001, Bonferroni post-hoc test). **e**. Working model schematics for SST$^+$ control analgesia induced during defensive states. Activation of SST$^+$ cells in the vlPAG is associated with the inhibition of fear-induced freezing behavior. Selective activation of RVM projecting SST$^+$ vlPAG cells is associated with inhibition of analgesia induced during defensive states.

Discussion

In this study, we established that SST$^+$ vlPAG cells control analgesia during defensive states in male mice. Endogenous pain-suppression was mediated by long-range SST$^+$ vlPAG cells projecting to the RVM, which, in turn, transmitted the pain signal to the DH of the spinal cord (Figures 2 and 5). Finally, our data indicated that SST$^+$ vlPAG cells can regulate both fear expression and the analgesia promoted during defensive states, and that the expression of these two behaviors can be segregated by precisely targeting the SST$^+$ vlPAG-RVM pathway (Figure 6). Together, these results identify a novel midbrain to brainstem circuit mechanism composed of long-range SST$^+$ vlPAG cells projecting to the RVM that regulate analgesia elicited during defensive states. Pain mechanisms and their modulation are known to exhibit sex-dependent differences[31], and thus we cannot exclude the possibility that the circuits described here may differ in females. Nevertheless, recent studies of RVM-spinal cord descending control suggest broadly similar organization and function across sexes[32,33]. Direct experimental investigation in female animals will be required to determine the extent to which the present findings generalize across sexes.

Our observations of the involvement of vlPAG in our cued-based fear conditioned analgesia paradigm are consistent with previous studies of contextual-based FCA involving this region[7]. In such FCA studies[6], animals undergo contextual fear conditioning followed by pain behavior testing in the same conditioning context, thereby limiting the temporally precise elicitation of aversive states. Instead, our behavioral paradigm goes beyond these limitations by promoting defensive states through a cued conditioned stimulus, advancing toward temporally specific manipulations such as optogenetics, and allowing us to study the phenomena with a within-subject experimental design through subsequent CS$^{+/-}$ presentations. Nevertheless, since the circuits involved in contextual and cued fear may differ[30,34], this might also imply different circuits involved in the emotional modulation of pain-suppression behavior. To our knowledge, this is the first demonstration of a cued fear-conditioned analgesia model in rodents. Addressing potential differences in the circuitry involved in contextual and cued fear-induced analgesia will require further investigation.

Our observation that photoactivation of SST$^+$ vlPAG cells not only abolished analgesia during defensive states but also decreased freezing expression has far-reaching functional consequences. Two independent previous studies found that long-range inhibitory inputs from the central medial amygdala contact inhibitory cells within the vlPAG, implicated in different roles: the modulation of fear behavior[23] and nociceptive transmission[35]. Notably, both studies describe the involvement of vlPAG inhibitory cells in a disinhibitory circuit mechanism of long-range projecting excitatory cells as the underlying neural substrates responsible for such modulations[23,35]. We observed that SST$^+$ cells are the most abundant inhibitory cell type in the vlPAG (Supplementary Figure 3). Thus, it is conceivable that the SST$^+$ vlPAG cells are indeed part of a circuit involved in the emotional regulation of endogenous pain-suppression. Notably, global manipulation of SST$^+$ vlPAG cells cannot disentangle their role in analgesia and fear behavior at the local level (Figures 2 and 3). Because the studies mentioned above exclusively addressed the contribution of vlPAG circuits to either pain[35] or fear[23] behavior, these studies may have been oblivious to alternative behavioral readout interpretations. Here, we demonstrated that SST$^+$ vlPAG cells projecting to the RVM modulate analgesia induced during defensive states without impacting the behavioral expression of fear (Figure 6). Thus, our results suggest that fear and analgesia signals rely on overlapping neuronal circuits and that the discrimination between these two states could be mediated within the vlPAG network. Altogether, our data are consistent with the existence of different populations of SST$^+$ cells within the vlPAG that mediate fear behavior and analgesic information, defined by their output connectivity.

The lateral inhibition model of analgesia within the PAG relies on the activation of PAG excitatory cells projecting to the RVM. More precisely, in this model, analgesia is thought to occur through an opioid-dependent inhibition of GABAergic cells, ultimately disinhibiting excitatory cells projecting to the RVM[12,20,21]. Our data indicate that, in addition to this disinhibitory mechanism, analgesia is also mediated by the inhibition of a direct long-range SST$^+$ neurons projection onto RVM cells

projecting to the DH (Figure 6). In line with this, inhibition of vlPAG SST cells induced analgesia in our experiments, consistent with previous findings obtained using chemogenetic approaches[36]. However, important differences emerge when comparing our results with Zhang et al.[34]. In that study, activation of vlPAG SST cells produced hyperalgesia, whereas in our study, activation of SST^+ vlPAG cells did not induce hyperalgesia but instead suppressed fear-conditioned analgesia. One key distinction between the two studies is the experimental context: Zhang et al. examined this circuit in a neuropathic pain model, whereas our work focuses on acute nociceptive processing and fear-dependent modulation of pain. Thus, the functional contribution of SST^+ vlPAG cells may depend on the behavioral and pathological state, with potentially distinct roles in chronic versus acute pain conditions[35]. In addition, methodological differences, such as our nociceptive test that uses a slow temperature ramp, may impose a floor effect that limits the detection of thermal hyperalgesia. Our results are therefore consistent with the parallel inhibition-excitation model, in which inhibitory and excitatory cells form two distinct, parallel descending pathways for pain modulation[24]. Indeed, previous studies have identified inhibitory projections within the PAG–RVM-spinal cord dorsal horn neuraxis[37], and our results suggest that SST^+ vlPAG cells contribute to analgesia within this broader framework. At the same time, our data indicate that vlPAG SST^+ cells are not exclusively inhibitory, as approximately one third co-localize with excitatory markers, and recent work has shown that excitatory SST^+ vlPAG cells project to the RVM[36]. Together, these observations raise the possibility that distinct SST^+ subpopulations contribute differently to descending pain control, with long-range vlPAG SST^+ cells participating in the excitatory pathway projecting throughout the PAG–RVM-spinal cord dorsal horn neuraxis, and local GABAergic vlPAG SST^+ cells contributing to local circuit dynamics related to fear response, such as freezing[23]. We identified a novel midbrain to brainstem circuit mechanism composed of SST^+ vlPAG cells that project to the RVM, thereby regulating analgesia during defensive states. Substantial progress has been made in outlining the midbrain circuitry of the endogenous pain-suppression pathway[12,24,26]. However, only more recently have high cortical areas been shown to be involved in analgesia[7,38]. Previous reports describe connections between CeL and vlPAG inhibitory neurons in the modulation of pain behavior[35,39]. Future work is required to elucidate whether the exact circuit that regulates analgesia is mediated by different negative emotional states, such as fear, depression, or stress.

Recent human reports reveal strong comorbidity between mood and anxiety disorders with and pain-related disorders[40], suggesting that the deregulation of the circuits mediating the interplay between emotional and pain behavior could be at the core of such psychiatric conditions. Comprehensive knowledge about the circuits mediating the emotional regulation of pain behavior is urgently needed. We identified an SST^+ cell type-and pathway-specific involvement in the mechanisms that mediate the emotion-dependent regulation of pain behavior. Thus, these findings may empower the development of more effective analgesic therapies by the improvement of further refined pharmacological targets.

Methods

Subject details

We used either male C57BL6/J mice (Janvier), heterozygous or homozygous Sst-IRES-Cre mice (Jackson laboratory), or heterozygous VIP-IRES-Cre mice (Jackson Laboratory) age 8-14 weeks, that were individually housed under a 12 h light-dark cycle and provided with food and water ad libitum. All procedures were performed in accordance with standard ethical guidelines (European Communities Directive 86/60-EEC) and were approved by the committee on Animal Health and Care of Institut National de la Santé et de la Recherche Médicale and the French Ministry of Agriculture and Forestry (agreement #A3312001).

Behavioral apparatus

Cued fear-conditioned analgesia *task* was performed in three different contexts (Figure 1a). Context A was used for *Habituation* and *Retrieval* and consisted of a plexiglass cylinder (25 x 24 cm diameter) with a grey, smooth plastic floor and house lights (16 lux). Context B was used for *Fear*

conditioning and consisted of a square plexiglass (25 x 40 cm) with a grid floor connected to a shocker (Coulbourn Instruments) and brighter house lights (40 lux). A total of 5 scrambled footshocks of 1 s duration and intensity of 0.8 mA were delivered via the grid floor and served as the unconditioned stimulus (US). Contexts A and B were cleaned, respectively, with 70% ethanol or 1 % acetic acid between different mice. Both contexts contained infrared beam detection that automatically scored freezing periods, determined by no change in infrared beam crossing for at least 2 s.

Context C was used for the *FC Hot Plate (HP) test*. A steady increase in temperature was controlled by the Incremental Hot/Cold Plate Analgesia Meter (IITC) device. To restrain the mice's movement, the HP apparatus had a testing surface (plate) enclosed in a square plexiglass surface (20.3 x 10 x 20.5 cm) and house lights (100 lux). The mice's temperature and surroundings were recorded using an infrared digital thermographic camera (Testo 885) placed ~ 50 cm above the testing surface. The thermal camera had a spatial resolution of 320 × 240 pixels, a sampling rate of 25 Hz, and thermal sensitivity of 0.03 °C at 30 °C. The testing surface of context C was cleaned with water between different mice. All three contexts were enclosed in an acoustic foam isolated box with speakers mounted on the top of each compartment. The auditory conditioned stimulus (CS) consists of either 7.5 kHz or white-noise 50 ms pips at 1 Hz, repeated 27 times, with 2 ms rise and fall, and a sound pressure level of 80 dB.

Open field *task* was performed in a square plexiglass arena (36 x 36 x 25cm). A LED mounted on the top-right side of the arena signaled the start and end of different epochs for offline analyses. A video camera recorded from above the arena at 30 fps for offline video-tracking purposes.

Real-Time Place Preference (RTPP) *task* was performed in a shuttlebox consisting of a plexiglass box (40 x 10 x 30 cm) with a floor grid, where a small plastic hurdle (1 cm height) divided the arena into two equal compartments, while infrared beam detection automatically monitored the mice shuttling between compartments (Imetronic). A video camera recorded from above the arena at 30 fps for offline video-tracking purposes.

For both the open field and RTPP tasks, a free user video-tracking software (idTracker: Tracking individuals in a group by automatic identification of unmarked animals) together with in-house codes in Matlab (The MathWorks, Inc., Natick, MA, USA) was used to analyze each condition.

Behavioral paradigm

Cued fear-conditioned analgesia (CFCA). C57BL6/J mice (n = 12) were habituated to the context and tones (day 1). Four white-noise (CS^-) and four 7.5 kHz (CS^+) tones were presented sequentially and without US reinforcement. In Fear conditioning (day 2), five CS^- and five CS^+ were presented in an intermingled fashion. The CS^+ presentations were paired with a mild footshock (US) at tone offset, whereas the CS^- was never reinforced. The Fear retrieval session (Day 3) was done 24h after conditioning and in the same context as the habituation session. As in habituation, four CS^- and four CS^+ were presented sequentially and without US reinforcement (Figure 1a).

Since the focus of this study was the emotional modulation of pain sensitivity, it was compulsory to evaluate the associative fear levels before measuring their impact on pain sensitivity. Two indices were computed: the discrimination index (DI), to assess the discrimination between $CS^-$and CS^+, and the conditioning index (CI), which indicated the level of freezing to the tone predicting the US. These indexes were calculated as follows: $\mathrm{DI} = \frac{(\text{Freezing to CS}+)-(\text{Freezing to CS}-)}{(\text{Freezing to CS}+)+(\text{Freezing to CS}-)}$ and CI = DI × (Freezing to CS^+). Based on preliminary data, mice were only submitted to the FC HP test if DI ≥ 0.4 & CI ≥ 0.3. Mice that did not fit the criteria were conditioned a second time. There was a minimum interval of 2 h between the retrieval and the FC HP test.

The FC HP test consisted of two trials, one in which the CS^+ was presented and another in which the CS^- was presented. The two trials were counterbalanced within the group. The testing surface was set at 30 °C. After a 60 s acclimatization period, its temperature gradually increased at 6 °C per minute (HP start). Tone presentation (CS^+ or CS^-) started 130 s after the HP start. Temperature increase and tone presentation terminated concomitantly with the display of a nociception response. Valid nociception readout responses included jumping or licking the hindpaw. The effect

of the negative emotional modulation on pain sensitivity was assessed by comparing the latency (or temperature) of the NC response between the two HP trials. There was a minimum of 30 min interval between the two trials for each mouse, during which mice returned to their home cage.

Freezing during the HP test was assessed by automatically analyzing thermographic camera videos using custom scripts (available at: *https://github.com/djercog/TestoFreez*). Briefly, individual video frames were binarized to define a mask for the mouse within each frame. Consecutive binarized frames were then subtracted, and the number of non-zero pixels in the resultant image determined if the mouse was considered immobile when below a certain threshold (defined to approximate manual freezing estimation on random videos). Immobilization episodes of at least 0.5 s were considered as freezing periods. In contrast, non-immobilization episodes shorter than 0.1 s were merged together with the neighbouring detected freezing episodes.

Extinction training. On days 3 and 4, mice (n =10) were submitted to an extinction training protocol established by Courtin et al. 2014[41]. Briefly, there were 4 CS^- and 12 CS^+, presented in a non-reinforced manner (Figure 1g). Mice were considered to have successfully extinguished the fear expression if the level of freezing in the last 4 CS^+ was not statistically different from the CS^-. After fear extinction, mice were submitted to the FC HP test, using the same parameters as in the CFCA paradigm.

Stability training. The first three days consisted of the classical CFCA paradigm. On day 4, mice (n = 10) repeated the protocol applied on day 3 (Supplementary Figure 2e-i). All mice that met the fear conditioning criteria (DI ≥ 0.4 & CI ≥ 0.3) on day 3 were kept for the following day, independent of their level of Conditioning on day 4.

Vasoconstriction assay. To determine whether vasoconstriction was a confounding factor in the FC HP test outcomes, we used a modified version of the CFCA paradigm (Figure 1f). During the HP test (n = 13), the temperature was not gradually increased but maintained at 30 °C while CSs were presented. The tones (CS^+ or CS^-) were presented for 120 s, and mice were kept for an additional 50 s before the HP trial terminated. Offline, with the infrared videos, mice's back and tail were measured at 30 s intervals. For each measurement point, the temperatures of three spots on the back and tail were averaged to obtain the body temperature for each body part at that time point and mouse.

Basal nociception assay (No tone). Naïve mice (n = 10) were submitted to the HP test (Figure 1i and Supplementary Figure 2a-d). Each mouse underwent two identical trials. The HP test was similar to the one described in the CFCA paradigm, except no tones were presented. There was a minimum of 30 min interval between the two trials, during which mice returned to a restful state in their home cage. Since the two trials were not significantly different, for simplicity, in panel i of Figure 1, the two trials were pooled together.

Tone-specific nociception assay. Naïve mice (n = 12) were submitted to the HP test without auditory fear conditioning (Figure 1i and Supplementary Figure 2a-d). Each animal underwent two trials, one trial with a 7.5 kHz tone presentation and another with a WN tone presentation. The tone presentation was counterbalanced. The HP test parameters were similar to those described for the CFCA, except that both tones were unconditioned. Since the two trials were not significantly different, for simplicity, in panel i of Figure 1, the two trials were pooled together.

Open Field assay. This test was used to determine the effect of optogenetic stimulation on locomotion. Therefore, only mice from optogenetic experiments were submitted to this assay. Mice could freely move during the entire test. The locomotion assay had a total duration of 9 min and was divided into 3 min epochs. The first and third epochs were OFF periods in which no optical stimulation occurred. During the second epoch, mice received photostimulation (ON period). The optogenetic stimulation effect was analyzed by comparing the overall distance traveled between the OFF and ON epochs (Supplementary Figure 5c, d). Mice injected with GFP were used to test

the effect of heat and light on the stimulation itself. Mouse tracking data were extracted from video recordings using idTracker[42] and imported into Matlab for further analysis with custom scripts to calculate the total distance traveled during stimulation.

Real-time Place Preference assay. Only mice from optogenetic experiments were submitted to this assay. During the entire duration of the assay, mice could freely shuttle between the two compartments. Under closed-loop stimulation, mice received photo-stimulation upon entry into one of the two compartments. The stimulated compartment was counterbalanced within the group. The optical stimulation effect was assessed by comparing the time spent in the stimulated compartment between the ChR2 and GFP groups (Supplementary Figure 5e, f). Permanence time in the stimulated compartment was automatically assessed by the apparatus software (Imetronic).

Virus injections and optogenetics

For optogenetic manipulation of SST^+ cells in the vlPAG, 0.15-0.2 µL of either ChR2 (AAV5-EF1a-DIO-hChR2(H134R)-EYFP, titer: 3.2×10^{12} - Vector Core, University of North Carolina), ArchT (AAV9-CAG-FLEX-ArchT-GFP, titer: 4.7×10^{12} - Vector Core, University of North Carolina) or GFP (AAV5-FLEX-GFP, titer: 4.5×10^{12} - Vector Core, University of North Carolina) were bilaterally injected into the vlPAG of 8/9 weeks old Sst-IRES-Cre mice from glass pipettes (tip diameter 20-30 µm) at the following coordinates relative to bregma: - 4.4 mm AP; ± 1.5 mm ML;-2.45 mm DV from dura, with a 20 degrees angle. Injection coordinates for manipulating VIP^+ vlPAG cells were as follows: - 4.4 mm AP; ± 1.35 mm ML;-2.5 mm DV from dura, with a 20 degrees angle.

At two weeks after the injections, mice were bilaterally implanted with custom-built optic fibers (diameter: 200 µm; numerical aperture: 0.39; Thorlabs) above the vlPAG at the following coordinates relative to bregma: i) Sst-IRES-Cre mice: - 4.4 mm AP; ± 1.0 mm ML;-1.8 mm DV from dura, with a 10 degrees angle; ii) VIP-IRES-Cre mice: - 4.4 mm AP; ± 0.8 mm ML;-2.0 mm DV from dura, with a 10 degrees angle. For RVM manipulations, mice were implanted at the following coordinates relative to bregma:-5.8 mm AP; 0.0 mm ML;-5.2 DV from the dura. All implants were secured using three stainless steel screws and Super-Bond cement (Sun Medical). During surgery, long-and short-lasting analgesic agents were injected (Metacam, Boehringer; Lurocaïne, Vetoquinol). After surgery, mice were allowed to recover for at least five days. Afterward, mice were handled daily to familiarize themselves with being restrained for the optic fibers connection. Behavioral experiments were performed at least four weeks after viral injections. Only mice with correct placement of optic fibers and virus expression were included in the analyses.

For optogenetic excitation, light stimulation consisted of blue light (473 nm, ~8-10 mW at fiber tip) delivered with 2 Hz frequency and 5 ms pulse duration. In contrast, light stimulation consisted of green light (532 nm, ~8-10 mW at fiber tip) delivered continuously for optogenetic inhibition. For optogenetic manipulations during the CFCA paradigm of either SST^+ or VIP^+ vlPAG cells, the light was delivered during the FC HP test and paired with the tone presentation.

Two sets of experiments were performed sequentially for stimulation during the fear conditioning. First, the footshock US was replaced by optical stimulation. Then, the US became the optical stimulation combined with the footshock (Supplementary Figure 6). For both conditions, optogenetic stimulation began 5 s before and lasted until 5 s after CS^+ offset. The same mice were used for both experiments. For the manipulations during the fear retrieval, there were 12 CS^+ presentations divided into blocks of 4 CS^+. The optogenetic stimulation was paired with the second block of CS^+.

Single-molecule *in situ* hybridization

Expression of *Sst*, *Slc31a1*, *Slc17a6,* and *Cre* transcripts was detected in C57/BL6J mice using single-molecule fluorescent *in situ* hybridization (smFISH) as previously described (Castell et al., 2024 PMID: 37858736). Briefly, coronal PAG sections (16 µm) were collected directly onto Superfrost Plus slides. Probes for *Sst* (ACDBio; Cat#404631), *Slc32a1* (ACDBio; Cat#319191-C2), *Slc17a6* (ACDBio; Cat#319171-C2), and *Cre* (ACDBio; Cat#312281-C2) were used with the RNAscope Fluorescent Multiplex Kit (ACDBio; Cat# 323110). Fluorescence was captured using sequential laser scanning confocal microscopy (Leica SP8), and quantification was performed in ImageJ.

Anatomical tracing

Fluorogold injection. An incision between one to two cm was made slightly caudal to the peak of the dorsal hump to expose the lumbar spinal region. The vertebra of interest was identified. Then, a small incision was made between the tendons and the vertebral column on either side. The vertebra was then secured using spinal adaptor clamps, and all tissue was removed from the surface of the bone. Pulled borosilicate glass capillaries (Ringcaps, disposable capillary pipettes with ring mark, DURAN, Hirschmann Laborgeräte, Germany) were inserted between 2 vertebrae and allowed to microinject 0.5 µL of fluorogold 2% in the dorsal horn of the spinal cord on both sides.

In vivo electrophysiology

Mice were anesthetized with isoflurane 4% for induction, then 1.5% maintenance. The experiment was started as soon as there was no longer any reflex. The colorectal temperature was kept at 37 °C with a heating blanket. Two metal clamps were used to stabilize the animal's spine in a stereotactic frame (M2E, France) during electrophysiological recordings. Then, a laminectomy was performed at T13-L1 to expose the lumbar part of the spinal cord. The dura mater was carefully removed. Custom-made optical fibers were placed 1mm above the dorsal spinal cord for optogenetic manipulations. C-fiber-evoked field potentials were recorded in the deep lamina of the DH (at a depth range of 250 and 500 µm) with borosilicate glass capillaries (2 MΩ, filled with NaCl 684 mM; Harvard Apparatus, Cambridge, MA, USA). Field potentials were recorded with an ISODAM-amplifier (low filter: 0.1Hz to high filter: 0.1 kHz; World Precision Instruments, USA) in response to electrical stimulation of the ipsilateral paw. Single unit recordings of WDR DH cells were made with the same borosilicate glass capillaries mentioned above and placed in the dorsal part of the spinal cord. The criterion for selecting a cell was the presence of an A-fiber-evoked response (0-80 ms) followed by a C-fiber-evoked response (80-150 ms) to electrical stimulation of the ipsilateral sciatic nerve.

The paw of the mice was stimulated by trains (every 30 s) of electrical stimulation at two times the threshold for C-fibers, which were performed before, during, and after optogenetic stimulations with an optic fiber placed above the recording site. Subthreshold stimulations were performed below the threshold for C-fiber and A-fiber, respectively.

Histology analyses

Mice were administered a lethal dose of Exagon and underwent transcardial perfusions via the left ventricle with 4% w/v paraformaldehyde (PFA) in 0.1 M PB. Following dissection, brains were post-fixed for 24 h at 4°C in 4% PFA. Brain sections of 80 µm-thick were cut on a vibratome, mounted on gelatin-coated microscope slides, and dried. To verify correct viral injections and optic fiber location, serial 80 µm-thick slices containing the regions of interest were mounted in VectaShield (Vector Laboratories) and imaged using an epifluorescence system (Leica DM 5000) fitted with a 10-x dry objective. The location and the extent of the injections/infections were visually controlled. Only infections targeting the vlPAG and optic fibers terminating, depending on the experiment, above the vlPAG or RVM were included in the analyses.

Statistics

All statistical details are contained in Supplementary Table 1. Box-whisker plots indicate median, interquartile range, and 5th - 95th percentiles of the distribution. All statistics are indicated where used. Statistical analyses were performed with Prism software (GraphPad). We tested the normality of all data with the Kolmogorov–Smirnov normality test in Prism software (GraphPad), and used nonparametric statistical tests for nonnormally distributed datasets, as indicated where used. No statistical methods were used to predetermine sample sizes, but sample sizes were based on previous studies in our laboratory. Blinding for the opsin was done for optogenetics experiments. Animals used for the CFCA paradigm that did not satisfy the DI and CI criteria after two conditioning sessions were discarded from the study. Mice with an incorrect injection of the opsins or misplaced location of the optic fibers were discarded. For *in vivo*

electrophysiology, field potentials were measured as the area above the curve in the C-fiber range (80-300 ms). Absolute values were used to compare values in each condition (OFF vs. ON optogenetic manipulation). In single-unit recordings, the number of A-and C-fiber induced spikes in WDR cells was measured after each electrical stimulation, during, and after optogenetic manipulation. An average of the four stimuli for each WDR recorded was used for statistical analysis. Outliers were removed using the Tukey method.

No other mice were excluded. Significance levels are indicated as follows: *p<0.05, **p<0.01, ***p<0.001, **** p<0.0001.

Supplementary figures

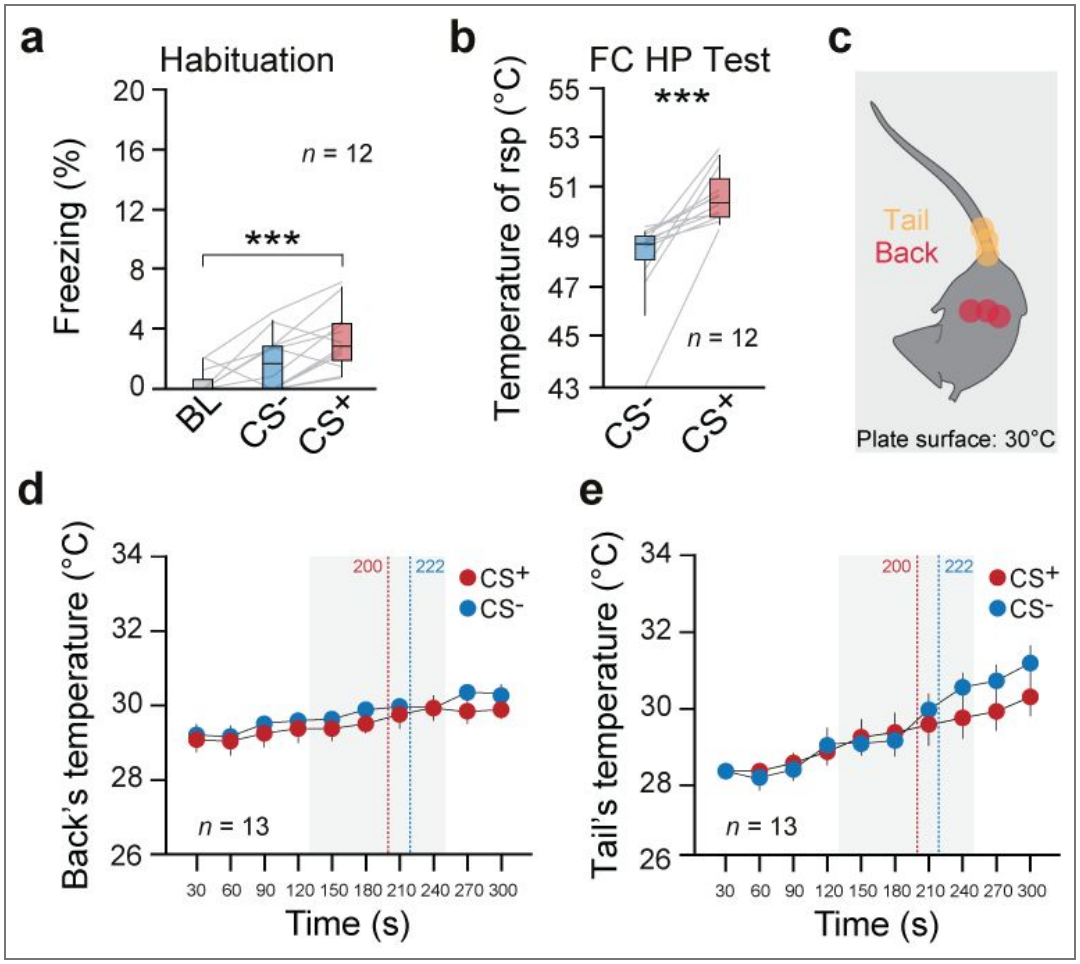

Supplementary Figure 1. Cued fear-conditioned analgesia behavior. a. During habituation, the freezing levels for the context (BL) and the two tones were low but significantly different (****, P = 0.0003, Friedman test, n = 12 mice). **b.** Mean temperature at which the NC response was observed in the HP test. The temperature of NC response was higher during CS^+ trials when compared to the CS^- trials (***, P = 0.0005, Wilcoxon matched-pairs signed rank test, n = 12 mice)**. c.** Schematic representation of how the back and tail temperature of the mice was measured. Every 30-sec three-point temperature was taken for each of the two body parts. The temperature of the mice back and tail were measured by the infrared digital thermographic camera and analyzed offline (see Methods). The average temperature of the mice back (**d**) and tail (**e**) while the CS^+ or the CS^- were presented. There were no differences in body temperature for the different CSs trials (ns, P > 0.05, mixed-effects model, n = 13 mice). Vertical dashed lines correspond to the average time of NC response for the CS^+ (red) and CS^- (blue) during the standard CFCA protocol.

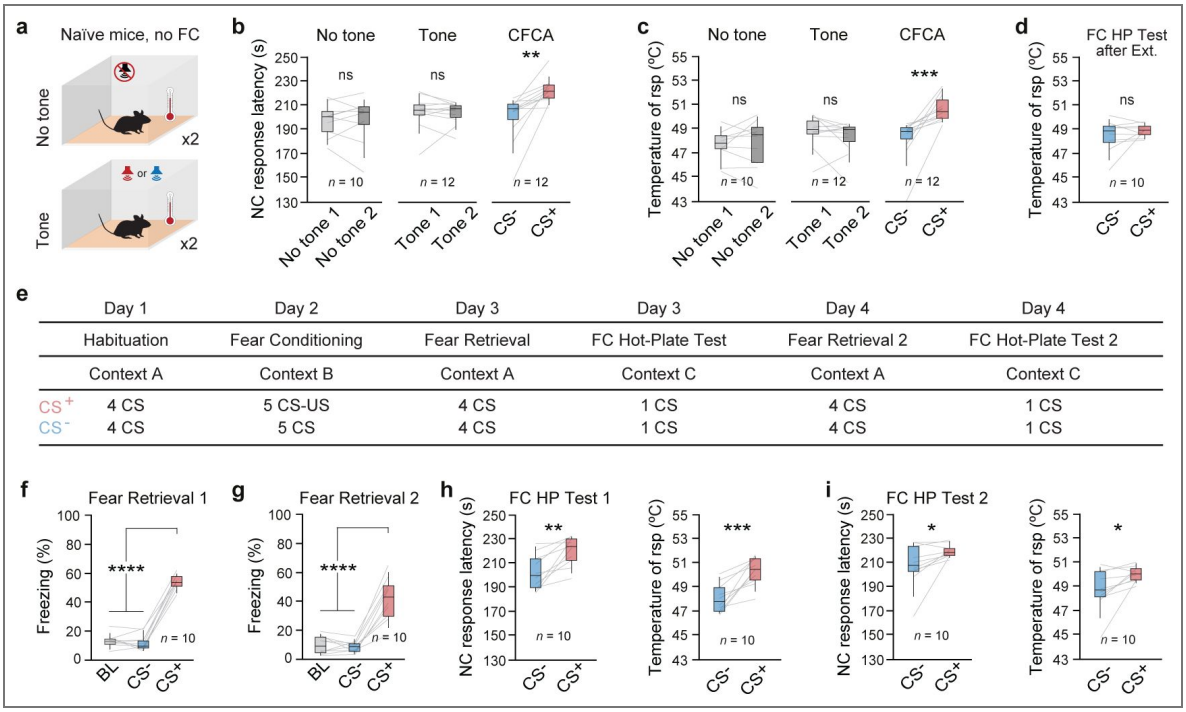

Supplementary Figure 2. CFCA depends on associative processes.

a. Top, protocol for the *No Tone*: naïve mice were submitted to two HP trials without conditioning nor tone presentation. **Bottom**, protocol for the *Tone*: naïve mice were submitted to two HP trials paired with an unconditioned tone presentation. **b, c.** Mean latency and temperature of NC response for the two tests mentioned above and the CFCA. The transient cued-fear induced analgesia (CS^+) compared to the basal nociception, the tone, and the CS^- trials (***, P = 0.0001, Krustal-Wallis test). Trials between the same type of test (*No tone* or *Tone*) were not significantly different (ns, P > 0.05, Bonferroni post-hoc test, see statistical table for all comparisons) **d.** After fear extinction, there was no difference in the mean temperature response between the two CSs (ns, P = 0.3276 paired t-test, n = 10 mice). **e.** Protocol for stability training (see methods). Mice were submitted to two rounds of the CFCA paradigm. During retrieval (**f, g**), average freezing values during CS^+ was higher than CS^- or baseline (BL) periods (****, P < 0.0001, one-way RM ANOVA, n = 10 mice). **h, i.** Mean latency and temperature of NC response during CS^- and CS^+ trials for FC HP test 1 (**h**) and test 2 (**i**). CS^+ presentation increased the latency and temperature of NC response in FC HP test 1 and test 2 (*, **, and ***, P < 0.05, paired t-test; for details, see Supplementary Table 1).

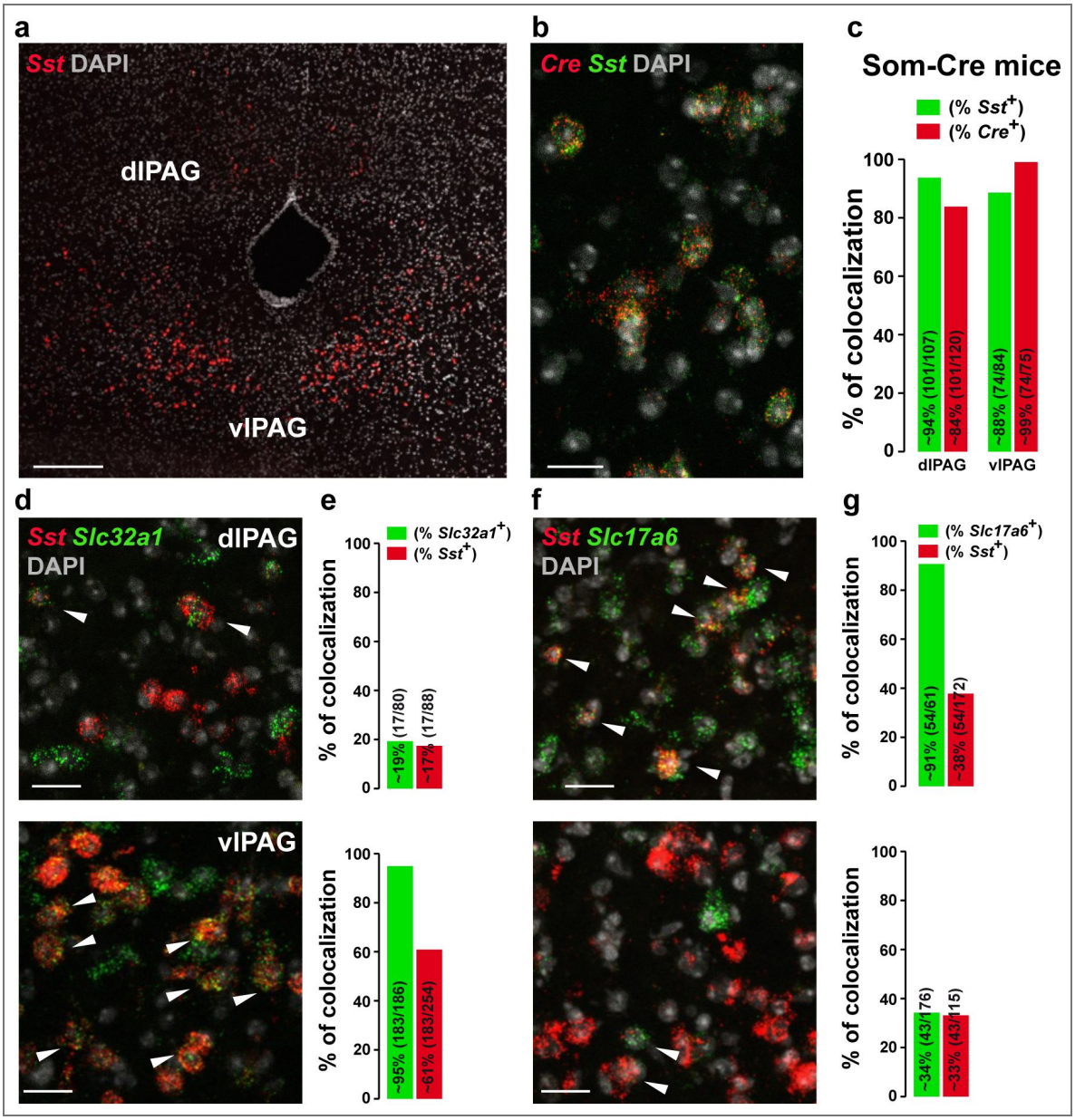

Supplementary Figure 3. Two distinct neuronal populations in SST-Cre mice within the PAG.

a. Representative picture of single-molecular fluorescent in situ hybridization for Sst mRNAs in the PAG. Scale bar, 400 µm. **b, c.** Single-molecular fluorescent in situ hybridization for Sst (green) and Cre (red) mRNAs in the vlPAG (left). Histograms showing the co-expression of Sst/Cre as percentage of Sst-expressing cells (green) and as percentage of Cre-expressing cells (red) in the dlPAG and vlPAG (right). Scale bar, 20 µm. In the dlPAG, 94% of RNA SST-expressing-cells (101 out of 107 cells) expressed Cre RNA, and 84 % of RNA Cre-expressing cells expressed somatostatin RNA (101 out of 20 cells). In the vlPAG, the values are 88% (74 out of 84 cells) and 99% (74 out of 75 cells) for Cre and SST, respectively. **d.** Single-molecular fluorescent in situ hybridization for Sst (red) and Slc32a1 (green) within the dlPAG (upper panel) and vlPAG (bottom panel). Scale bar, 20 µm. **e.** Quantification of colocalization within the dlPAG (upper panel) and vlPAG (bottom panel) of Sst^+ and $Slc32a1^+$. In the dlPAG, approximately 19% of $Slc32a1^+$ cells (17 out of 80 cells) are Sst^+, and 17% (17 out of 88 cells) of Sst^+ cells are $Slc32a1^+$. On the contrary, in the vlPAG, approximately 95% of $Slc32a1^+$ cells (183 out of 186 cells) are Sst^+, and 61% of Sst^+ cells (183 out of 254 cells) are $Slc32a1^+$. **f.** Single-molecular fluorescent in situ hybridization for Sst (red) and Slc17a6 (green) within the dlPAG (upper panel) and vlPAG (bottom panel). Scale bar, 20 µm. **g.** Quantification of colocalization within the dlPAG (upper panel) and vlPAG (bottom panel) of Sst^+ and $Slc17a6^+$. In the dlPAG, approximately 91% of $Slc17a6^+$ cells (54 out of 61 cells) are Sst^+, and 38% of Sst^+ cells (54 out of 172 cells) are $Slc17a6^+$. On the contrary, in the vlPAG, approximately 34% of $Slc17a6^+$ cells (43 out of 176 cells) are Sst^+ and 33% of Sst^+ cells (43 out of 115 cells) are $Slc17a6^+$. White arrows indicate colocalization.

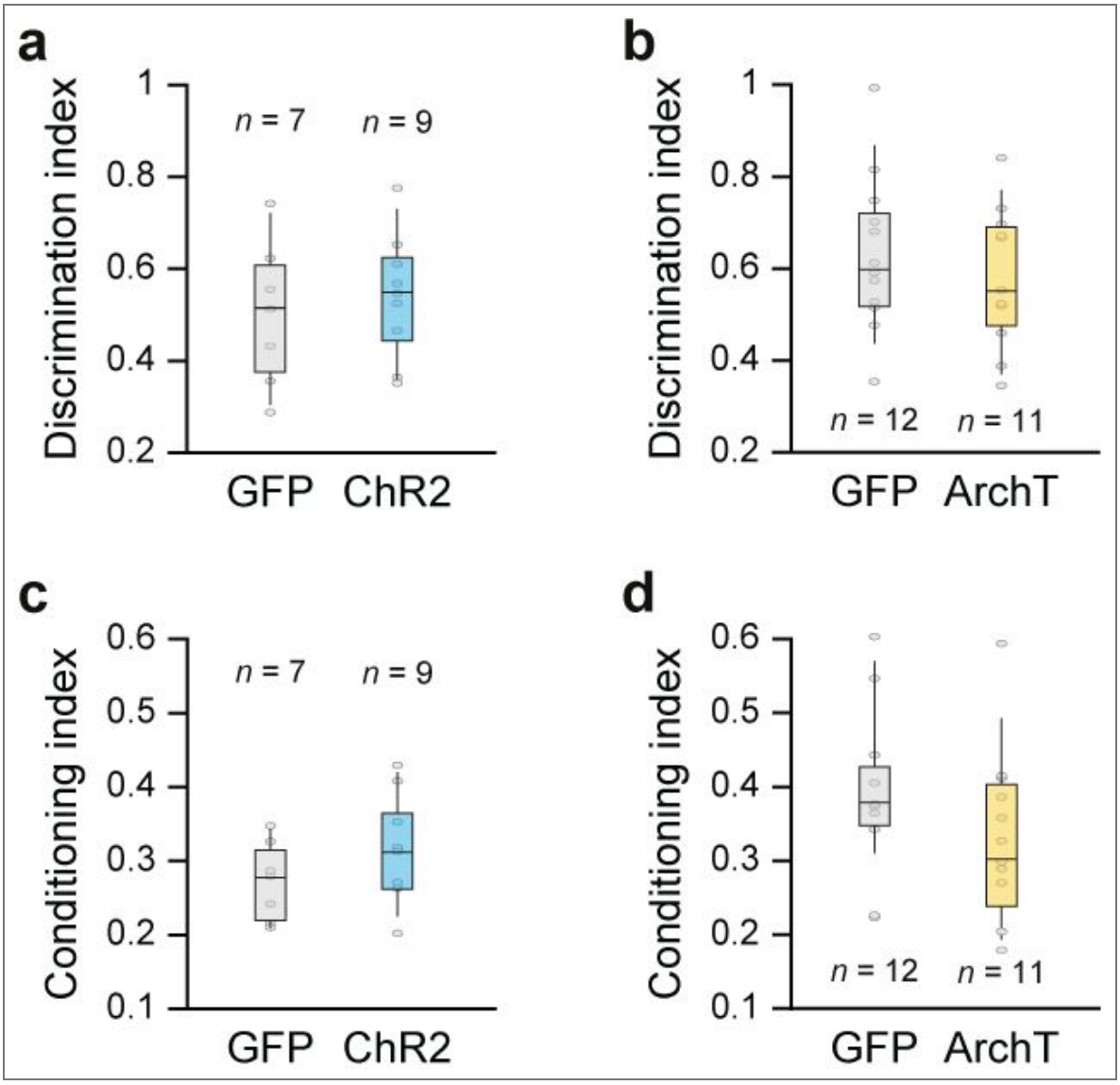

Supplementary Figure 4. Comparable fear levels prior to the FC HP test.

After retrieval, fear conditioning levels between the opsins and their respective GFP groups were tested to ensure equivalent fear levels. The discrimination index (see methods) between the GFP and ChR2 (**a**, ns, P = 0.6052 unpaired t-test, n = 16 mice) or ArchT (**b,** ns, P = 0.4575, unpaired t-test, n = 23 mice) were not significantly different. All the mice discriminated equally between CSs. The conditioning index (see methods) between the GFP and ChR2 (**c,** ns, P = 0.2333, unpaired t-test n = 16 mice) or ArchT (**d,** ns, P = 0.1320, unpaired t-test, n = 23 mice) were also not significantly different. All mice displayed a similar high freezing level to the CS^{+}.

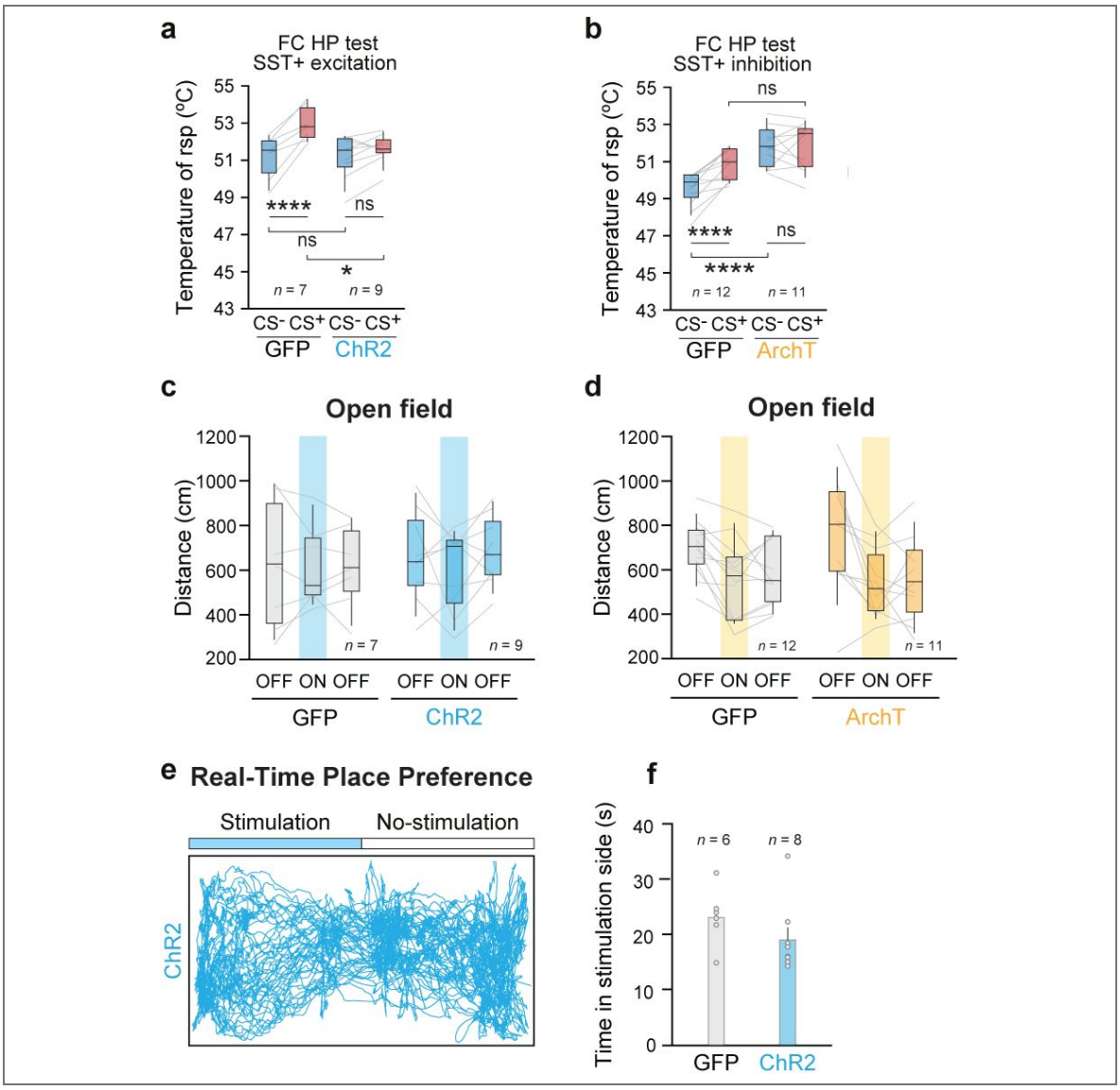

Supplementary Figure 5. Optogenetic manipulation of SST$^+$ vlPAG cells does not affect locomotion or produce aversion.

a. Photoactivation of SST$^+$ vlPAG cells abolished the analgesic effect induced during defensive states (**, P = 0.0035, opsin x CS - two-way RM ANOVA, n = 7 GFP, n = 9 ChR2). The mean temperature of NC response for the CS$^+$ was significantly different between the ChR2 and GFP groups (*, P = 0.0322, Bonferroni post-hoc test). For the ChR2 group, the mean temperature of NC response during CS$^+$ was equivalent to the CS$^-$ (ns, P = 0.1783, Bonferroni post-hoc test). On the contrary, the mean temperature of NC response between the CSs differed for the GFP group (****, P < 0.0001, Bonferroni post-hoc test). **b.** Photoinhibition of SST$^+$ vlPAG cells increased the analgesic effect for the ArchT group when compared to the GFP (**, P = 0.0035, opsin x CS - two-way RM ANOVA, n = 12 GFP, n = 11 ArchT). The mean temperature of NC response for the CS$^-$ was significantly different between the ArchT and GFP groups (****, P < 0.0001, Bonferroni post-hoc test). For the GFP group, the mean temperature of NC response was higher for the CS$^+$ trials when compared to the CS$^-$ trials (***, P = 0.0003, Bonferroni post-hoc test), yet this was not the case for the ArchT group (ns, P > 0.999, Bonferroni post-hoc test). **c.** The photoactivation of SST$^+$ vlPAG cells was performed during the ON epoch (blue shaded area), and the average distance traveled during the ON epoch was not different from the OFF epochs when comparing the two opsins (ns, P = 0.5121, opsin x light - two-way RM ANOVA, n = 7 GFP, n = 9 ChR2). **d.** The photoinhibition of SST$^+$ vlPAG cells was performed during the ON epoch (yellow shaded area), and the average distance traveled during the ON epoch was not different from the OFF epochs when comparing the two opsins (ns, P =0.4047, opsin x light - two-way RM ANOVA, n = 12 GFP, n = 11 ArchT). **e.** Real-time place-preference location plot from a representative animal while submitted to optogenetic activation of SST$^+$ vlPAG cells in the left compartment throughout the 15-min session. **f.** There was no difference between ChR2-expressing mice and the control group in the time spent in the stimulated and non-stimulated compartments (ns, P = 0.1812, Mann-Whitney test).

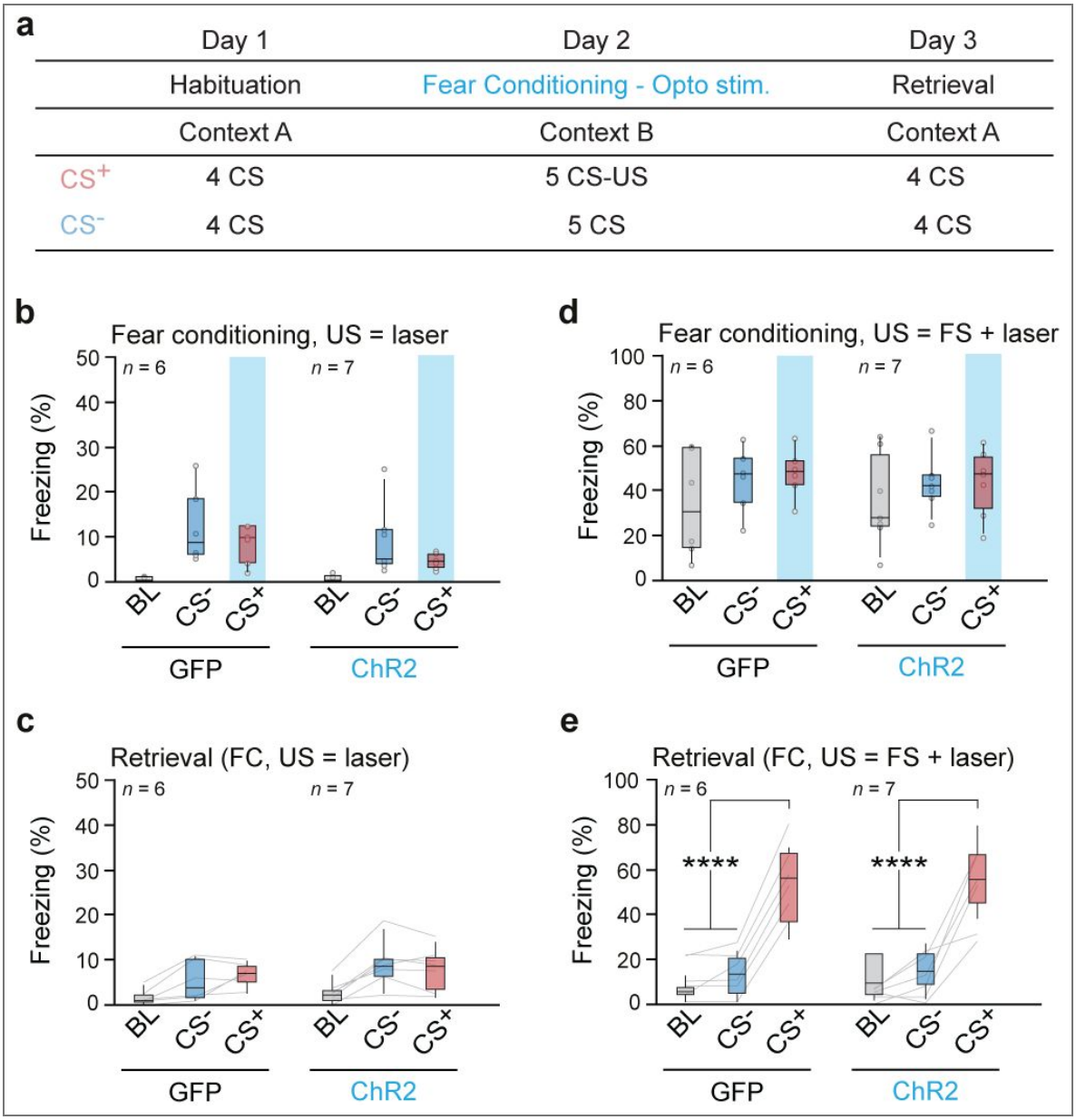

Supplementary Figure 6. SST$^+$ vlPAG cells photoactivation during conditioning does not impact fear learning.

a. Protocol for optogenetic manipulations during fear conditioning. On Day 2, mice received 5 CS-US associations. The US was either optogenetic stimulation alone or optogenetic stimulation plus footshock. **b.** Average freezing levels during the CS-US association of optogenetic stimulation alone. There was no difference in the overall freezing levels for the CS$^-$and CS$^+$ between ChR2 and GFP (ns, P = 0.4804, opsin x CS - two-way RM ANOVA, n = 6 GFP, n = 7 ChR2). **c.** During retrieval, there was no effect on freezing upon activation of SST$^+$ vlPAG cells as an US (ns, P = 0.4804, opsin x CS effect - two-way RM ANOVA, n = 6 GFP, n = 7 ChR2). **d.** Average freezing levels during the CS-US association of optogenetic stimulation plus footshock. There was no difference in the overall freezing levels for the CS$^+$ and CS$^-$ between ChR2 and GFP (ns, P = 0.8663, opsin x CS effect - two-way RM ANOVA, n = 6 GFP, n = 7 ChR2). **e.** During retrieval, there was no difference in the fear expression by the activation of the SST$^+$ vlPAG cells (ns, P = 0.8967, opsin x CS effect - two-way RM ANOVA, n = 6 GFP, n = 7 ChR2).

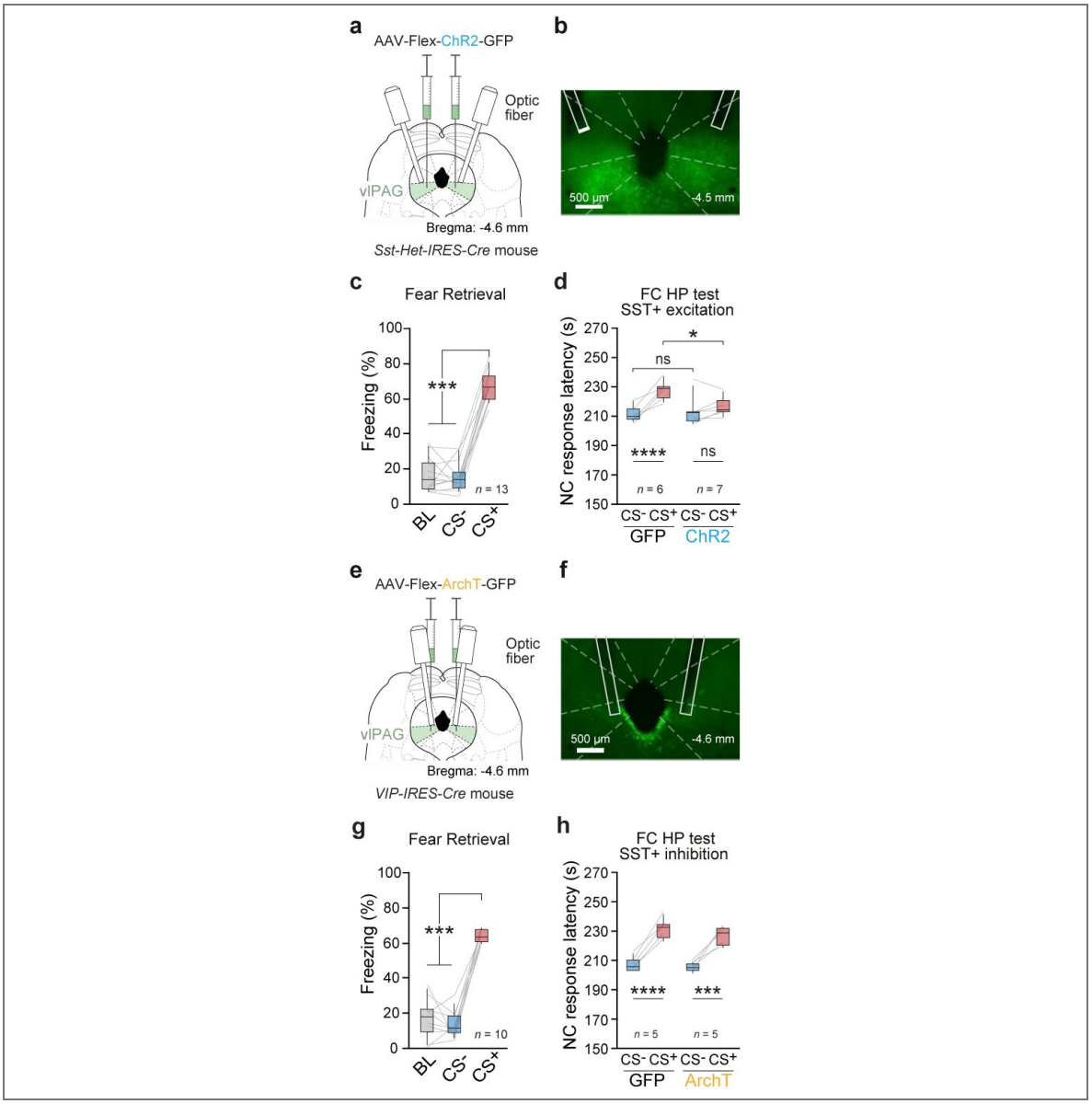

Supplementary Figure 7. Optogenetic effect observed during CFCA is not due to alteration of somatostatin levels nor mediated by VIP$^+$ vlPAG cells.

a. Sst-IRES-Cre heterozygotic mice received a bilateral injection of opsins in the vlPAG, and optic fibers were implanted above the vlPAG. **b.** A representative example of expression patterns of ChR2 within SST$^+$ vlPAG cells. **c.** Average freezing values during retrieval. ChR2 and GFP groups were pooled together because no differences were found in the conditioning level (data not shown). The average freezing values during CS$^+$ were higher than CS$^-$ or baseline (BL) periods (****, P < 0.0001, Friedman test, n = 13 mice). **d.** Optogenetic activation of SST$^+$ vlPAG cells abolished the analgesic effect induced by defensive states (**, P = 0.0048, opsin x CS - two-way RM ANOVA, n = 6 GFP, n = 7 ChR2). The mean latency of NC response for the CS$^+$ was significantly different between the ChR2 and GFP groups (*, P = 0.0300, Bonferroni post-hoc test, n = 6 GFP, n = 7 ChR2). For the ChR2 group, the latency of NC response during CS$^+$ was equivalent to the CS$^-$ (ns, P = 0.3342, Bonferroni post-hoc test). On the contrary, the latency of NC response between the CSs was different for the GFP group (****, P = 0.0001, Bonferroni post-hoc test). **e.** VIP-IRES-Cre mice received a bilateral injection of opsins in the vlPAG, and optic fibers were implanted above the vlPAG. **f.** Representative example of the expression pattern of ArchT within VIP$^+$ vlPAG cells. **g.** ArchT and GFP groups were pooled together because no differences were found in the conditioning level (data not shown). The average freezing values during CS$^+$ were higher than CS$^-$ or BL periods (****, P < 0.0001, one-way RM ANOVA, n = 10 mice). **h.** Optogenetic inhibition of VIP$^+$ cells did not change the analgesic effect for the ArchT group when compared to the GFP (ns, P = 0.5455, opsin x CS effect - two-way RM ANOVA, n = 5 GFP, n = 5 ArchT). The latency of NC response was higher for the CS$^+$ trials compared to the CS$^-$ trials for both GFP and ArchT (***, P < 0.01, Bonferroni post-hoc test, n = 5 GFP, n = 5 ArchT).

Supplementary Figure 8. Optogenetic activation of SST$^+$ vlPAG cells did not affect tactile sensitivity.

a. Perievent stimulus time histogram indicating the spiking latency of a purely tactile neuron recorded in the spinal cord in response to gentle brushing of the skin. **b.** Representative spiking activity latency of a purely tactile neuron recorded in the spinal cord in response to gentle brushing of the skin with or without activation of ChR2 expressing SST$^+$ vlPAG cells. **c.** The activation of ChR2 expressing SST$^+$ vlPAG cells of tactile neurons recorded in the spinal cord in response to gentle brushing of the skin had no effect on the average firing activity (Paired t-test, P = 0.6929, n = 5 cells).

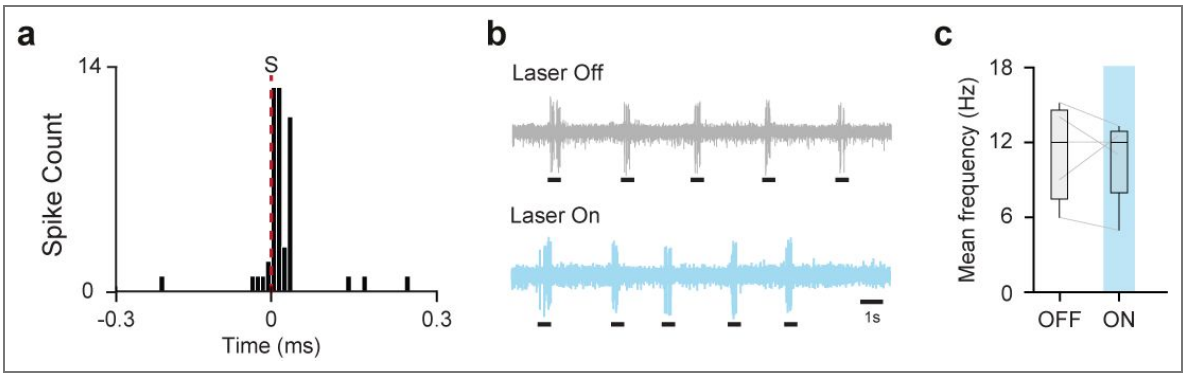

Supplementary Figure 9. Optogenetic manipulation of GFP expressing vlPAG cells did not affect analgesia.

a. Single-unit recordings of WDR cells in the lumbar spinal cord during optogenetic manipulation of GFP expressing SST$^+$ vlPAG inputs to the RVM. **b**. Photostimulation of SST$^+$ vlPAG inputs to the RVM has no effect.

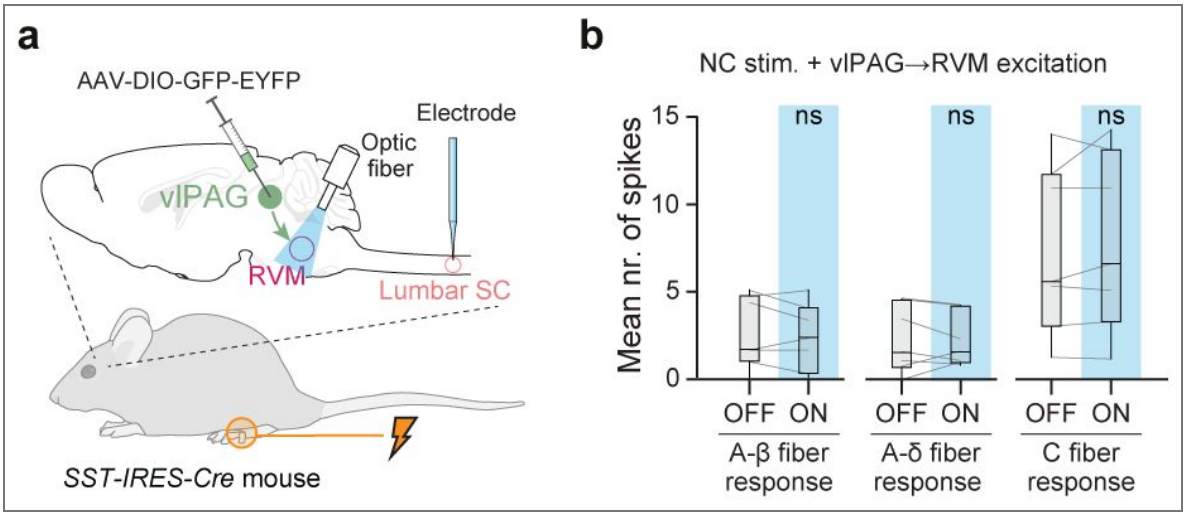

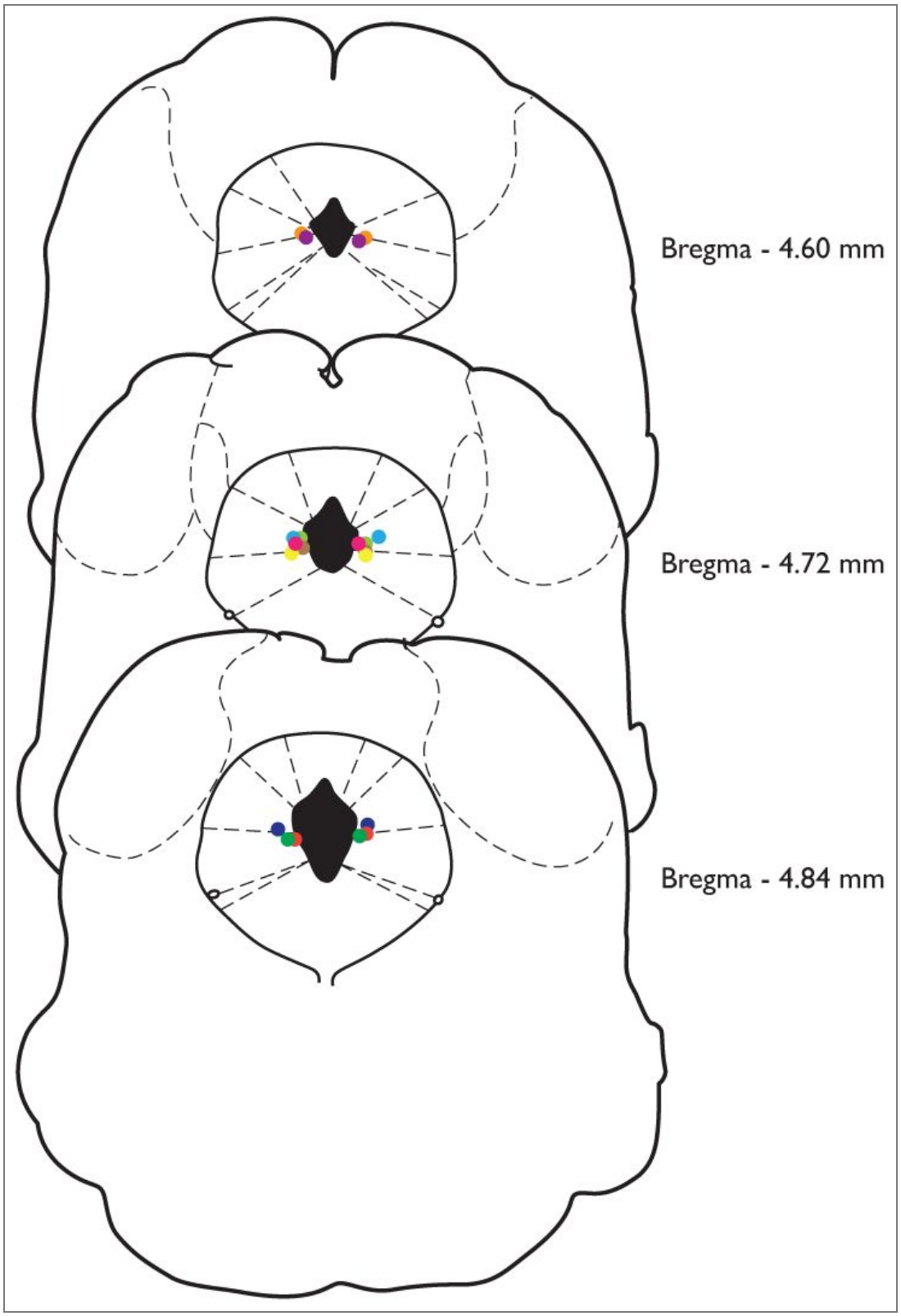

Supplementary Figure 10. Optical fiber placement for VIP-Cre.

Anatomical location of the tip of the optic fiber for VIP-Cre mice (n = 10).

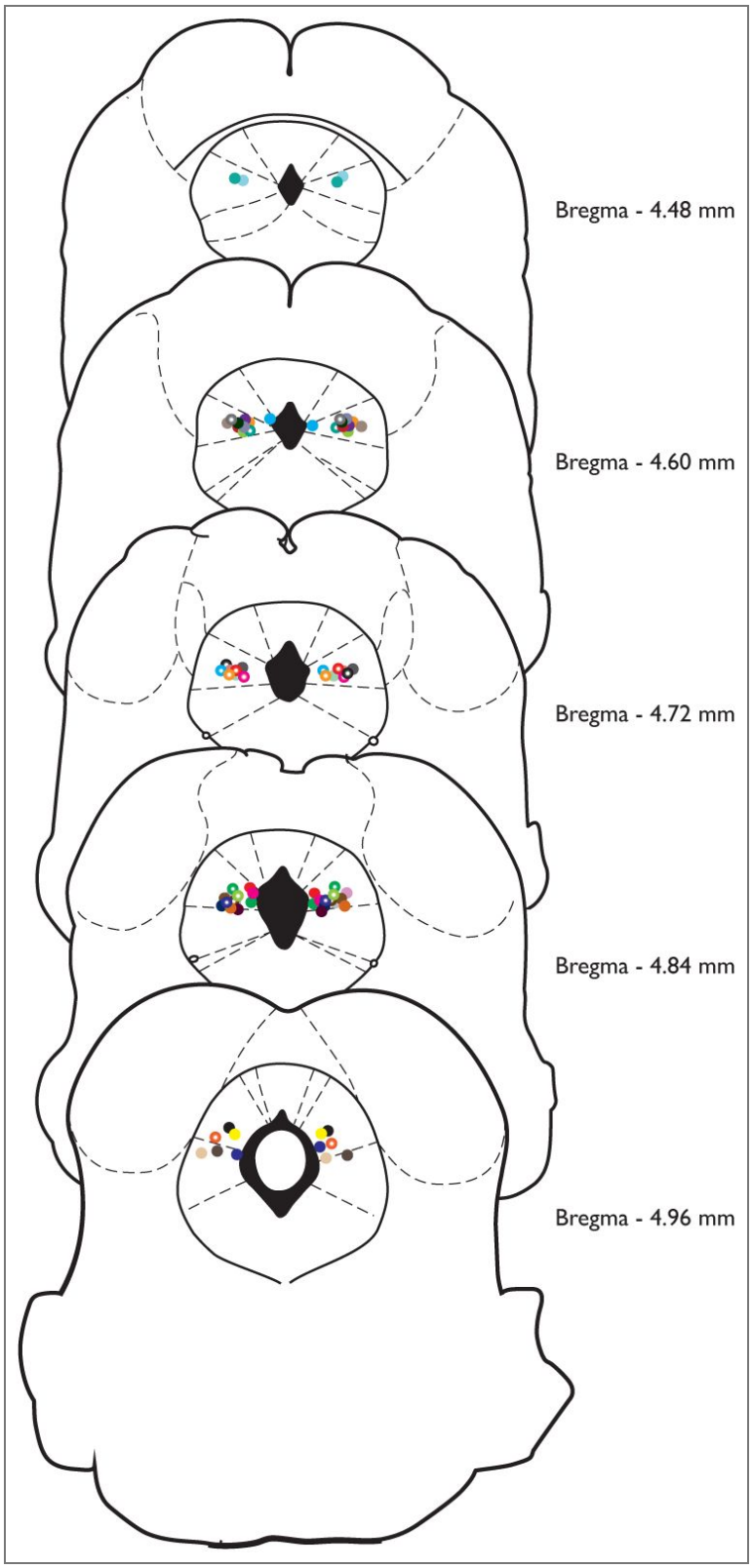

Supplementary Figure 11. Optical fiber placement for SST-Cre mice.

Anatomical location of the tip of the optic fiber for SST-Cre mice (n = 39).

Supplementary table

Figure number	Normality test	Statistic method	Main effect	Post hoc multiple comparisons test	Number of mice	Number of cells
1b	Passed	One-way RMA NOVA followed by Bonferroni post-hoc test	$F_{(2, 22)} = 160.8$ P value < 0,0001	BL vs. CS^-, P > 0.9999, ns BL vs. CS^+, P < 0,0001 CS^- vs. CS^+, P < 0,0001	12	NA
1e	Failed	Wilcoxon matched-pairs signed rank test (two-tailed)	P = 0.0005	$W = 78.00$	12	NA
1f	Onset, failed Offset, failed	Wilcoxon matched-pairs signed rank test (two-tailed)	Onset, P = 0.0015 Offset, P = 0.8330, ns	Onset, $W = 74$ Offset, $W = 6$	12	NA
1g	Failed	Friedman test followed by Dunn's multiple post-hoc test	P value < 0,0001 $Q = 48.13$	BL vs. CS^-, P > 0.9999, ns BL/CS^- vs. $CS^+_{1st\ block}$, P < 0,0001 CS^- vs. $CS^+_{5th/6th\ block}$, P > 0.9999, ns $CS^+_{1st\ block}$ vs. $CS^+_{5th/6th\ block}$, P < 0.005	10	NA
1h	Passed	Paired t-test (two-tailed)	P = 0.4365, ns	$t_9 = 0.8143$	10	NA
1i	Failed	Krustal-Wallis test followed by Dunn's multiple post-hoc test	P < 0.0001 $H = 25.32$	No tone vs. Tone, P = 0.7710, ns No tone vs. CS^-, P > 0.9999, ns Tone vs. CS^-, P > 0.9999, ns No tone vs. CS^+, P < 0.0001 Tone vs. CS^+, P = 0.0009 CS^- vs CS^+, P = 0.0033	No tone = 10 Tone = 12 CSs =12	NA
2c	Passed	One-way RM ANOVA followed by Bonferroni post-hoc test	$F_{(2,30)} = 396.8$ P < 0.0001	BL vs. CS^-, P > 0.9999, ns BL vs. CS^+, P < 0,0001 CS^- vs. CS^+, P < 0,0001	16	NA
2d	Passed	Two-way RM ANOVA followed by Bonferroni post-hoc test	Opsin x CS, $F_{(1,14)} = 8.514$ P = 0.0112	CS^- vs. CS^+, GFP, P = 0.0003 CS^- vs. CS^+, ChR2, P = 0.3876, ns GFP vs. ChR2, CS^-, P > 0.9999, ns GFP vs. ChR2, CS^+, P = 0.0344	GFP = 7 ChR2 = 9	NA
2e	Passed	One-way RM ANOVA followed by Bonferroni post-hoc test	$F_{(2,44)} = 280.4$ P < 0.0001	BL vs. CS^-, P = 0.2337, ns BL vs. CS^+, P < 0,0001 CS^- vs. CS^+, P < 0,0001	23	NA
2f	Passed	Two-way RM ANOVA followed by Bonferroni post-hoc test	Opsin x CS, $F_{(1,21)} = 10.64$ P = 0.0037	CS^- vs. CS^+, GFP, P = 0.0003 CS^- vs. CS^+, ArchT, P > 0.9999, ns GFP vs. ArchT, CS^-, P < 0,0001 GFP vs. ArchT, CS^+, P = 0.0265	GFP = 12 ArchT = 11	NA
3c	Passed	Two-way RM ANOVA followed by Bonferroni post-hoc test	Opsin x CS, $F_{(4,48)} = 0.1954$ P = 0.9396, ns	BL vs. CS^-, GFP/ArchT, P > 0.9999, ns BL vs. $CS^+_{1st/2nd/3rd}$, GFP/ArchT, P < 0,0001 CS^- vs. $CS^+_{1st/2nd/3rd}$, GFP/ArchT, P < 0,0001 CS^+_{1st} vs. $CS^+_{2nd/3rd}$, GFP/ArchT, P > 0.9999, ns CS^+_{2nd} vs. CS^+_{3rd}, GFP/ArchT, P > 0.9999, ns GFP vs. ArchT, BL/CS^-/$CS^+_{1st/2nd/3rd}$, P > 0.9999, ns	GFP = 6 ArchT = 8	NA
3d	Passed	Two-way RM ANOVA followed by Bonferroni post-hoc test	Opsin x CS, $F_{(4,60)} = 7.957$ P < 0.0001	BL vs. CS^-, GFP/ChR2, P > 0.9999, ns BL vs. $CS^+_{1st/2nd/3rd}$, GFP, P < 0,0001 CS^- vs. $CS^+_{1st/2nd/3rd}$, GFP, P < 0,0001 CS^+_{1st} vs. $CS^+_{2nd/3rd}$, GFP, P > 0.9999, ns CS^+_{2nd} vs. CS^+_{3rd}, GFP, P > 0.9999, ns BL vs. $CS^+_{1st/3rd}$, ChR2, P < 0,0001 BL vs. CS^+_{2nd}, ChR2, P = 0.0789, ns CS^- vs. $CS^+_{1st/3rd}$, ChR2, P < 0,0001 CS^- vs. CS^+_{2nd}, ChR2, P > 0.9999, ns CS^+_{1st} vs. CS^+_{2nd}, ChR2, P < 0,0001 CS^+_{1st} vs. CS^+_{3rd}, ChR2, P = 0.2372, ns CS^+_{2nd} vs. CS^+_{3rd}, ChR2, P < 0,0001 GFP vs. ChR2, BL/CS-/$CS^+_{1st/3rd}$, P > 0.9999, ns GFP vs. ChR2, CS^+_{2nd}, P = 0.0002	GFP = 9 ChR2 = 8	NA
4b	Passed	One-way RM ANOVA followed by Bonferroni post-hoc test	$F_{(2, 14)} = 17,94$ P = 0,0001	OFF1 vs. ON, P = 0.0006 OFF2 vs. ON, P = 0.0003 OFF1 vs. OFF2, P > 0.9999, ns	8	NA
4c	Passed	One-way RM ANOVA followed by Bonferroni post-hoc test	$F_{(2, 8)} = 5,826$ P = 0,0275	OFF1 vs. ON, P = 0.0414 OFF2 vs. ON, P = 0.0452 OFF1 vs. OFF2, P = 0.9980, ns	5	NA
4d	A-β fiber, passed A-δ fiber, passed C fiber, passed	Paired t-test (two-tailed)	A-β fiber, P = 0.5430, ns A-δ fiber, P = 0.0022 C fiber, P = 0.0033	A-β fiber, $t_{11} = 0.6319$ A-δ fiber, $t_{11} = 3.959$ C fiber, $t_{11} = 3.739$	8	A-β fiber,11 A-δ fiber, 11 C fiber, 11
4e	A-β fiber, passed A-δ fiber, passed C fiber, passed	Paired t-test (two-tailed)	A-β fiber, P = 0.1386, ns A-δ fiber, P = 0.0241 C fiber, P < 0.0001	A-β fiber, $t_{13} = 1.578$ A-β fiber, $t_{13} = 2.553$ C fiber, $t_{13} = 6.274$	5	A-β fiber,14 A-δ fiber, 14 C fiber, 14
4f	A-β fiber, failed A-δ fiber, failed C fiber, failed	Wilcoxon matched-pairs signed rank test (two-tailed)	A-β fiber, P = 0.3750, ns A-δ fiber, P = 0.0156 C fiber, P = 0.0020	A-β fiber, $W = 7.0$ A-β fiber, $W = 28.0$ C fiber, $W = 55.0$	8	A-β fiber,10 A-δ fiber, 10 C fiber, 10
5e	Passed	Paired t-test (two-tailed)	P = 0.3683, ns	$t_{10} = 0.94222$	7	11

5f, left	A-β fiber, passed A-δ fiber, passed C fiber, failed	Paired t-test (two-tailed) Paired t-test (two-tailed) Wilcoxon matched-pairs signed rank test (two-tailed)	A-β fiber, P = 0.0740, ns A-δ fiber, P = 0.0346 C fiber, P = 0.0020	A- β fiber, t_9 = 2.021 A-δ fiber, t_9 = 2.487 C fiber, W = 55.0	7	A-β fiber,10 A-δ fiber, 10 C fiber, 10
5f, right	Failed	Wilcoxon matched-pairs signed rank test (two-tailed)	P = 0.0078	W = 36.0	7	9
6b	Passed	Two-way RM ANOVA followed by Bonferroni post-hoc test	Opsin x CS, $F_{(4,44)}$ = 0.6292 P = 0.6443, ns	BL vs. CS^- GFP/ChR2, P > 0.9999, ns BL vs. $CS^+_{1st/2nd/3rd}$, GFP/ChR2, P < 0,0001 CS^- vs. $CS^+_{1st/2nd/3rd}$, GFP/ChR2, P < 0,0001 CS^+_{1st} vs. CS^+_{2nd}, GFP/ChR2, P > 0.9999, ns CS^+_{2nd} vs. CS^+_{3rd}, GFP/ChR2, P > 0.9999, ns CS^+_{1st} vs. CS^+_{3rd}, GFP, P = 0.0090 CS^+_{1st} vs. CS^+_{3rd}, ChR2, P = 0.0003 GFP vs. ChR2, BL/CS^-/$CS^+_{1st/2nd/3rd}$, P > 0.9999, ns	GFP = 7 ChR2 = 6	NA
6c	Passed	One-way RM ANOVA followed by Bonferroni post-hoc test	$F_{(2,26)}$ = 274.2 P < 0.0001	BL vs. CS^-, P > 0.9999, ns BL vs. CS^+, P < 0,0001 CS^- vs. CS^+, P < 0,0001	14	NA
6d	Passed	Two-way RM ANOVA followed by Bonferroni post-hoc test	Opsin x CS, $F_{(1,12)}$ = 10.91 P = 0.0063	CS^- vs. CS^+ - GFP, P < 0,0001 CS^- vs. CS^+ - ChR2, P > 0.9999, ns GFP vs. ChR2 – CS^-, P = 0.5378, ns GFP vs. ChR2 – CS^+, P = 0.0002	GFP = 7 ChR2 = 7	NA
Supp1a	Failed	Friedman test followed by Dunn's multiple post-hoc test	P = 0.0003 Q = 16.55	BL vs. CS^-, P = 0.3074, ns BL vs. CS^+, P = 0.0003 CS^- vs. CS^+, P = 0.0742, ns	12	NA
Supp1b	Failed	Wilcoxon matched-pairs signed rank test (two-tailed)	P = 0.0005	W = 78.0	12	NA
Supp1d	Passed	Mixed-effects model followed by Bonferroni post-hoc test	CS x Time, $F_{(9,238)}$ = 0.1716 P = 0.9967	CS^+ vs. CS^- for each time point, all P > 0.9999, ns	13	NA
Supp1e	Passed	Mixed-effects model followed by Bonferroni post-hoc test	CS x Time, $F_{(9,238)}$ = 0.7147 P = 0.6952	CS^+ vs. CS^- for each time point, all P > 0.9999, ns	13	NA
Supp2b	No tone, passed Tone, passed CFCA, failed	Paired t-test (two-tailed) Paired t-test (two-tailed) Wilcoxon matched-pairs signed rank test (two-tailed)	No tone, P = 0.9866, ns Tone, P = 0.9085, ns CFCA, P = 0.0005	No tone, t_9 = 0.01732 Tone, t_{11} = 0.1176 CFCA, W = 78.0	No tone= 10 Tone = 12 CFCA =12	NA
Supp2b	Failed	Krustal-Wallis test followed by Dunn's multiple post-hoc test	P = 0.0001 H = 25.45	No tone 1 vs. No tone 2/Tone 1/Tone 2/CS-, P > 0.9999, ns No tone 2 vs. Tone 1/Tone 2/CS-, P > 0.9999, ns Tone 1 vs. Tone 2/CS-, P > 0.9999, ns Tone 2 vs. Tone CS-, P > 0.9999, ns No tone 1 vs. CS+, P = 0.0002 No tone 2 vs. CS+, P = 0.0009 Tone 1 vs. CS+, P = 0.0178 Tone 2 vs. CS+, P = 0.0133 CS- vs. CS+, P =0.0082	No tone = 10 Tone = 12 CFCA =12	NA
Supp2c	No tone, passed Tone, failed CFCA, failed	Paired t-test (two-tailed) Wilcoxon matched-pairs signed rank test (two-tailed)	No tone, P = 0.6216, ns Tone, P = 0.4375, ns CS, P = 0.0005	No tone, t_9 = 0.5111 Tone, W = -21.0 CFCA, W = 78.0	No tone = 10 Tone = 12 CFCA =12	NA
Supp2c	Failed	Krustal-Wallis test followed by Dunn's multiple post-hoc test	P < 0.0001 H = 29.30	No tone 1 vs. No tone 2/Tone 1/Tone 2/CS^-, P > 0.9999, ns No tone 2 vs. Tone 1/Tone 2/CS^-, P > 0.9999, ns Tone 1 vs. Tone 2/CS-, P > 0.9999, ns Tone 2 vs. Tone CS^-, P > 0.9999, ns No tone 1 vs. CS^+, P < 0.0001 No tone 2 vs. CS^+, P = 0.0010 Tone 1 vs. CS^+, P = 0.0339 Tone 2 vs. CS^+, P = 0.0037 CS^- vs. CS^+, P =0.0033	No tone = 10 Tone = 12 CFCA =12	NA
Supp2d	Passed	Paired t-test (two-tailed)	P = 0.3276, ns	t_9 = 1.035	10	NA
Supp2f	Passed	One-way RM ANOVA followed by Bonferroni post-hoc test	$F_{(2,18)}$ = 558.2 P < 0.0001	BL vs. CS^-, P > 0.9999, ns BL vs. CS^+, P < 0,0001 CS^- vs. CS^+, P < 0,0001	10	NA
Supp2g	Passed	One-way RM ANOVA followed by Bonferroni post-hoc test	$F_{(2,18)}$ = 56.00 P < 0.0001	BL vs. CS^-, P > 0.9999, ns BL vs. CS^+, P < 0,0001 CS^- vs. CS^+, P < 0,0001	10	NA
Supp2h, left	Passed	Paired t-test (two-tailed)	P = 0.0029	t_9 = 4.054	10	NA
Supp2h, right	Passed	Paired t-test (two-tailed)	P = 0.0006	t_9 = 5.184	10	NA
Supp2i, left	Passed	Paired t-test (two-tailed)	P = 0.0362	t_9 = 2.459	10	NA

Supp2i, right	Passed	Paired t-test (two-tailed)	P = 0.0245	$t_9 = 2.697$	10	NA
Supp4a	Passed	Unpaired t-test (two-tailed)	P = 0.6052	$t_{14} = 0.5288$	GFP = 7 ChR2 = 9	NA
Supp4b	Passed	Unpaired t-test (two-tailed)	P = 0.4575	$t_{21} = 0.7569$	GFP = 12 ArchT = 11	NA
Supp4c	Passed	Unpaired t-test (two-tailed)	P = 0.2333	$t_{14} = 1.246$	GFP = 7 ChR2 = 9	NA
Supp4d	Passed	Unpaired t-test (two-tailed)	P = 0.1320	$t_{21} = 1.567$	GFP = 12 ArchT = 11	NA
Supp5a	Passed	Two-way RM ANOVA followed by Bonferroni post-hoc test	Opsin x CS, $F_{(1,14)} = 11.40$ P = 0.0045	CS^- vs. CS^+, GFP, P < 0,0001 CS^- vs. CS^+, ChR2, P = 0.1783, ns GFP vs. ChR2, CS^-, P > 0.9999, ns GFP vs. ChR2, CS^+, P = 0.0322	GFP = 7 ChR2 = 9	NA
Supp5b	Passed	Two-way RM ANOVA followed by Bonferroni post-hoc test	Opsin x CS, $F_{(1,21)} = 10.84$ P = 0.0035	CS^- vs. CS^+, GFP, P = 0.0003 CS^- vs. CS^+, ArchT, P > 0.9999, ns GFP vs. ArchT, CS^-, P < 0,0001 GFP vs. ArchT, CS^+, P = 0.0704, ns	GFP = 12 ArchT = 11	NA
Supp5c	Passed	Two-way RM ANOVA followed by Bonferroni post-hoc test	Opsin x Light, $F_{(2,28)} = 0.6855$ P = 0.5121, ns	OFF_1 vs. ON, GFP/ChR2, P > 0.9999, ns OFF_2 vs. ON, GFP/ChR2, P > 0.9999, ns OFF_1 vs. OFF_2, GFP/ChR2, P > 0.9999, ns GFP vs. ChR2, OFF_1/ON/OFF_2, P > 0.9999, ns	GFP = 7 ChR2 = 9	NA
Supp5d	Passed	Two-way RM ANOVA followed by Bonferroni post-hoc test	Opsin x Light, $F_{(2,42)} = 0.9243$ P = 0.4047, ns	OFF_1 vs. ON, GFP, P = 0.0165 OFF_1 vs. ON, ArchT, P = 0.0003 OFF_2 vs. ON, GFP/ArchT P > 0.9999, ns OFF_1 vs. OFF_2, GFP/ArchT, P > 0.9999, ns GFP vs. ArchT, OFF_1/ON/OFF_2, P > 0.9999, ns	GFP = 12 ArchT = 11	NA
Supp5f	Failed	Mann Whitney test (two-tailed)	P = 0.1812	$U = 13$	GFP = 6 ChR2 = 8	NA
Supp6b	Passed	Two-way RM ANOVA followed by Bonferroni post-hoc test	Opsin x CS, $F_{(2,22)} = 0.7582$ P = 0.4804, ns	GFP vs. ChR2, BL/CS^-/CS^+, P > 0.9999, ns	GFP = 6 ChR2 = 7	NA
Supp6c	Passed	Two-way RM ANOVA followed by Bonferroni post-hoc test	Opsin x CS, $F_{(2,22)} = 1.926$ P = 0.1695, ns	GFP vs. ChR2, BL/CS^-/CS^+, P > 0.9999, ns	GFP = 6 ChR2 = 7	NA
Supp6d	Passed	Two-way RM ANOVA followed by Bonferroni post-hoc test	Opsin x CS, $F_{(2,22)} = 0.1444$ P = 0.8663, ns	GFP vs. ChR2, BL/CS^-/CS^+, P > 0.9999, ns	GFP = 6 ChR2 = 7	NA
Supp6e	Passed	Two-way RM ANOVA followed by Bonferroni post-hoc test	Opsin x CS, $F_{(2,22)} = 0.1095$ P = 0.8967, ns	GFP vs. ChR2, BL/CS^-/CS^+, P > 0.9999, ns BL vs. CS^-, GFP, P > 0.9999, ns BL vs. CS^-, ChR2, P > 0.5328, ns BL vs. CS^+, GFP/ChR2, P < 0.0001 CS^- vs. CS^+, GFP/ChR2, P < 0.0001	GFP = 6 ChR2 = 7	NA
Supp7c	Failed	Friedman test followed by Dunn's multiple post-hoc test	P value < 0.0001 $Q = 19.85$	BL vs. CS^-, P > 0.9999, ns BL vs. CS^+, P = 0,0012 CS^- vs. CS^+, P = 0,0001	13	NA
Supp7d	Passed	Two-way RM ANOVA followed by Bonferroni post-hoc test	Opsin x CS, $F_{(1,11)} = 12.39$ P = 0.0048	CS^- vs. CS^+, GFP, P = 0.0001 CS^- vs. CS^+, ChR2, P = 0.3342, ns GFP vs. ChR2, CS^-, P > 0.9999, ns GFP vs. ChR2, CS^+, P = 0.0300	GFP = 6 ChR2 = 7	NA
Supp7g	Passed	One-way RM ANOVA followed by Bonferroni post-hoc test	$F_{(2,18)} = 147.1$ P < 0.0001	BL vs. CS^-, P = 0.8655, ns BL vs. CS^+, P < 0,0001 CS^- vs. CS^+, P < 0,0001	10	NA
Supp7h	Passed	Two-way RM ANOVA followed by Bonferroni post-hoc test	Opsin x CS, $F_{(1,8)} = 0.3984$ P = 0.5455, ns	CS^- vs. CS^+, GFP, P = 0.0001 CS^- vs. CS^+, ArchT, P = 0.0003 GFP vs. ChR2, CS^-, P > 0.9999, ns GFP vs. ChR2, CS^+, P = 0.3869, ns	GFP = 5 ArchT = 5	NA
Supp8c	Passed	Paired t-test (two-tailed)	P = 0.6929, ns	$t_4 = 0.4247$	5	5
Supp9b	A-β fiber, passed A-δ fiber, passed C fiber, passed	Paired t-test (two-tailed)	A-β fiber, P = 0.3750, ns A-δ fiber, P = 0.7369, ns C fiber, P = 0.4150, ns	A- β fiber, $t_6 = 0.9564$ A-δ fiber, $t_6 = 0.3520$ C fiber, $t_6 = 0.8755$	3	A-β fiber, 7 A-δ fiber, 7 C fiber, 7

Supplementary Table 1. Summary of statistical results associated with the Figures and Supplementary Figures

Data availability

Data supporting the findings of this study, including analysis codes, are available from the corresponding author upon request.

Acknowledgements

We thank Joshua Johansen, David Finn, and Nadine Gogolla for critical and stimulating discussions; K. Deisseroth and E. Boyden for generously sharing material, S. Laumond, J. Tessaire, and the technical staff of the housing and experimental animal facility of the Neurocentre Magendie. We thank Claire Francioni for her technical support. Microscopy was performed in the Bordeaux Imaging Center of the CNRS-INSERM and Bordeaux University, member of France BioImaging. This work was supported by grants from the French National Research Agency (ANR-FEARLESSPAIN, ANR-10-EQPX-08 OPTOPATH), the Fondation pour la Recherche Médicale (FRM-PhD grant to NW 2020-2021) and the French Society for the Study and Treatment of Pain (SFETD – grant to NW 2022).

Additional information

Author Contributions

N.W performed behavioral experiments and optogenetic experiments on freely moving animals.

F.A, J.V, performed electrophysiological and optogenetic experiments on anesthetized animals. E.V, L.C, N.W, F.A, Z.G, C.R, R.B, and D.G performed histology. N.W, M.L, S.V. P.F, and C.H. designed the experiments. N.W, F.A, D.J, and E.V analyzed the data, N.W, D.J. and C.H wrote the paper.

Funding

Funder	Grant reference number	Author
Agence Nationale de la Recherche (ANR)	ANR-19-CE16-0016	Cyril Herry Fossat Pascal
Agence Nationale de la Recherche (ANR)	ANR-23-CE37-0015	Cyril Herry Fossat Pascal
Agence Nationale de la Recherche (ANR)	ANR-10-EQPX-08-optopath	Cyril Herry
Fondation pour la Recherche Médicale (FRM)	FRM-PhD	Nanci Winke

Author ORCID iDs

Coline Riffault: https://orcid.org/0009-0005-1580-3265
Cyril Herry: https://orcid.org/0000-0003-2973-0843

References

1. **Bolles RC,** Fanselow MS (1980) A perceptual-defensive-recuperative model of fear and pain. *Behav. Brain Sci* **3**:291-301 https://doi.org/10.1017/s0140525x0000491x
2. **Rhudy JL,** Meagher MW (2000) Fear and anxiety: divergent effects on human pain thresholds. *Pain* **84**:65-75 https://doi.org/10.1016/s0304-3959(99)00183-9 | PubMed
3. **Flor H,** Grösser SM (1999) Conditioned stress-induced analgesia in humans. *Eur. J. Pain* **3**:317-324 https://doi.org/10.1053/eujp.1999.0137 | PubMed
4. **Beckham JC,** et al. (1997) Chronic posttraumatic stress disorder and chronic pain in Vietnam combat veterans. *J. Psychosom. Res* **43**:379-389 https://doi.org/10.1016/s0022-3999(97)00129-3 | PubMed
5. **International Association for the Study of Pain** (2017) IASP Terminology. IASP.

6. **Butler RK,** Finn DP (2009) Stress-induced analgesia. *Prog. Neurobiol* **88**:184-202 https://doi.org/10.1016/j.pneurobio.2009.04.003 | PubMed
7. **Rea K,** Roche M, Finn DP (2011) Modulation of Conditioned Fear, Fear-Conditioned Analgesia, and Brain Regional C-Fos Expression Following Administration of Muscimol into the Rat Basolateral Amygdala. *J. Pain* **12**:712-721 https://doi.org/10.1016/j.jpain.2010.12.010 | PubMed
8. **Floyd NS,** Price JL, Ferry AT, Keay KA, Bandler R (2000) Orbitomedial prefrontal cortical projections to distinct longitudinal columns of the periaqueductal gray in the rat. *J. Comp. Neurol* **422**:556-578 https://doi.org/10.1002/1096-9861(20000710)422:4<556::aid-cne6>3.0.co;2-u | PubMed
9. **LeDoux J,** Iwata J, Cicchetti P, Reis D (1988) Different projections of the central amygdaloid nucleus mediate autonomic and behavioral correlates of conditioned fear. *J. Neurosci* **8**:2517-2529 https://doi.org/10.1523/jneurosci.08-07-02517.1988 | PubMed
10. **Vertes RP** (2004) Differential projections of the infralimbic and prelimbic cortex in the rat. *Synapse* **51**:32-58 https://doi.org/10.1002/syn.10279 | PubMed
11. **Carrive P,** Morgan MM (2012) Chapter 10 - Periaqueductal Gray. In: Mai JK, Paxinos G (Eds). *The Human Nervous* **631** Elsevier. pp. 367-400 https://doi.org/10.1016/B978-0-12-374236-0.10010-0
12. **Basbaum AI,** Fields HL (1984) Endogenous Pain Control Systems: Brainstem Spinal Pathways and Endorphin Circuitry. *Annu. Rev. Neurosci* **7**:309-338 https://doi.org/10.1146/annurev.ne.07.030184.001521 | PubMed
13. **Millan MJ** (2002) Descending control of pain. *Prog. Neurobiol* **66**:355-474 https://doi.org/10.1016/s0301-0082(02)00009-6 | PubMed
14. **Fields HL,** Heinricher MM, Mason P (1991) Neurotransmitters in Nociceptive Modulatory Circuits. *Annu. Rev. Neurosci* **14**:219-245 https://doi.org/10.1146/annurev.ne.14.030191.001251 | PubMed
15. **Samineni VK,** et al. (2017) Divergent Modulation of Nociception by Glutamatergic and GABAergic Neuronal Subpopulations in the Periaqueductal Gray. *eneuro* **4**:ENEURO.0129-16.2017 https://doi.org/10.1523/eneuro.0129-16.2017 | PubMed
16. **Castilho V,** Macedo C, Brandão M (2002) Role of benzodiazepine and serotonergic mechanisms in conditioned freezing and antinociception using electrical stimulation of the dorsal periaqueductal gray as unconditioned stimulus in rats. *Psychopharmacology (Berl.)* **165**:77-85 https://doi.org/10.1007/s00213-002-1246-4 | PubMed
17. **Helmstetter FJ,** Landeira-Fernandez J (1990) Conditional hypoalgesia is attenuated by Naltrexone applied to the periaqueductal gray. *Brain Res* **537**:88-92 https://doi.org/10.1016/0006-8993(90)90343-a | PubMed
18. **Bellgowan PSF,** Helmstetter FJ (1998) The role of mu and kappa opioid receptors within the periaqueductal gray in the expression of conditional hypoalgesia. *Brain Res* **791**:83-89 https://doi.org/10.1016/s0006-8993(98)00057-2 | PubMed
19. **Jacquet YF** (1988) The NMDA receptor: central role in pain inhibition in rat periaqueductal gray. *Eur. J. Pharmacol* **154**:271-276 https://doi.org/10.1016/0014-2999(88)90201-4 | PubMed
20. **Moreau JL,** Fields HL (1986) Evidence for GABA involvement in midbrain control of medullary neurons that modulate nociceptive transmission. *Brain Res* **397**:37-46 https://doi.org/10.1016/0006-8993(86)91367-3 | PubMed
21. **Osborne PB,** Vaughan CW, Wilson HI, Christie MJ (1996) Opioid inhibition of rat periaqueductal grey neurones with identified projections to rostral ventromedial medulla in vitro. *J. Physiol* **490**:383-389 https://doi.org/10.1113/jphysiol.1996.sp021152 | PubMed
22. **Harris JA** (1996) Descending antinociceptive mechanisms in the brainstem: Their role in the animal's defensive system. *J. Physiol-Paris* **90**:15-25 https://doi.org/10.1016/0928-4257(96)87165-8
23. **Tovote P,** et al. (2016) Midbrain circuits for defensive behaviour. *Nature* **534**:206-212 https://doi.org/10.1038/nature17996 | PubMed
24. **Lau BK,** Vaughan CW (2014) Descending modulation of pain: the GABA disinhibition hypothesis of analgesia. *Curr. Opin. Neurobiol* **29**:159-164 https://doi.org/10.1016/j.conb.2014.07.010 | PubMed

25. **Fields H** (2004) State-dependent opioid control of pain. *Nat. Rev. Neurosci* **5**:565-575 https://doi.org/10.1038/nrn1431 | PubMed

26. **Ossipov MH,** Dussor GO, Porreca F (2010) Central modulation of pain. *J. Clin. Invest* **120**:3779-3787 https://doi.org/10.1172/jci43766 | PubMed

27. **Vianna DML,** Carrive P (2005) Changes in cutaneous and body temperature during and after conditioned fear to context in the rat. *Eur. J. Neurosci* **21**:2505-2512 https://doi.org/10.1111/j.1460-9568.2005.04073.x | PubMed

28. **Smith GST,** et al. (1994) Distribution of messenger RNAs encoding enkephalin, substance P, somatostatin, galanin, vasoactive intestinal polypeptide, neuropeptide Y, and calcitonin gene-related peptide in the midbrain periaqueductal grey in the rat. *J. Comp. Neurol* **350**:23-40 https://doi.org/10.1002/cne.903500103 | PubMed

29. **Viollet C,** et al. (2017) Somatostatin-IRES-Cre Mice: Between Knockout and Wild-Type?. *Front. Endocrinol* **8** https://doi.org/10.3389/fendo.2017.00131 | PubMed

30. **Gasser HS** (1941) The classification of nerve fibers. *Ohio J. Sci*

31. **Mogil JS** (2012) Sex differences in pain and pain inhibition: multiple explanations of a controversial phenomenon. *Nat. Rev. Neurosci* **13**:859-866 https://doi.org/10.1038/nrn3360 | PubMed

32. **Aby F,** et al. (2022) Switch of serotonergic descending inhibition into facilitation by a spinal chloride imbalance in neuropathic pain. *Sci. Adv* **8**:eabo0689 https://doi.org/10.1126/sciadv.abo0689 | PubMed

33. **Grivet Z,** et al. (2025) Brainstem serotonin amplifies nociceptive transmission in a mouse model of Parkinson's disease. *Npj Park. Dis* **11** https://doi.org/10.1038/s41531-024-00857-1 | PubMed

34. **Tovote P,** Fadok JP, Lüthi A (2015) Neuronal circuits for fear and anxiety. *Nat. Rev. Neurosci* **16**:317-331 https://doi.org/10.1038/nrn3945 | PubMed

35. **Yin W,** et al. (2020) A Central Amygdala–Ventrolateral Periaqueductal Gray Matter Pathway for Pain in a Mouse Model of Depression-like Behavior. *Anesthesiology* **132**:1175-1196 https://doi.org/10.1097/aln.0000000000003133 | PubMed

36. **Zhang Y,** et al. (2023) Somatostatin Neurons from Periaqueductal Gray to Medulla Facilitate Neuropathic Pain in Male Mice. *J. Pain* **24**:1020-1029 https://doi.org/10.1016/j.jpain.2023.01.002 | PubMed

37. **Morgan MM,** Whittier KL, Hegarty DM, Aicher SA (2008) Periaqueductal gray neurons project to spinally projecting GABAergic neurons in the rostral ventromedial medulla. *Pain* **140**:376-386 https://doi.org/10.1016/j.pain.2008.09.009 | PubMed

38. **Butler RK,** et al. (2011) Molecular and electrophysiological changes in the prefrontal cortex–amygdala–dorsal periaqueductal grey pathway during persistent pain state and fear-conditioned analgesia. *Physiol. Behav* **104**:1075-1081 https://doi.org/10.1016/j.physbeh.2011.05.028 | PubMed

39. **Tovote P,** Esposito MS, Botta P, Chaudun F, Jonathan P (2016) Midbrain circuits for defensive behaviour. *Nat. Press* https://doi.org/10.1038/nature17996 | PubMed

40. **McWilliams LA,** Cox BJ, Enns MW (2003) Mood and anxiety disorders associated with chronic pain: an examination in a nationally representative sample. *Pain* **106**:127-133 https://doi.org/10.1016/s0304-3959(03)00301-4 | PubMed

41. **Courtin J,** et al. (2014) Prefrontal parvalbumin interneurons shape neuronal activity to drive fear expression. *Nature* **505**:92-6 https://doi.org/10.1038/nature12755 | PubMed

42. **Pérez-Escudero A,** Vicente-Page J, Hinz RC, Arganda S, De Polavieja GG (2014) idTracker: tracking individuals in a group by automatic identification of unmarked animals. *Nat. Methods* **11**:743-748 https://doi.org/10.1038/nmeth.2994 | PubMed

Peer reviews

Reviewer #1 (Public review):

[Editors' note: this version has been assessed by the Reviewing Editor without further input from the original reviewers. The authors have addressed the comments raised in the previous round of review.]

Summary:

In the manuscript by Winke et al, the authors present evidence that fear-induced analgesia is mediated by somatostatin projection cells from the vlPAG to the RVM. This study uses a mouse model of fear-induced analgesia, and incorporates optogenetic circuit manipulation with behaviour and electrophysiology to gain a meaningful insight into a novel circuit involved in fear-induced analgesia.

Strengths:

(1) This is a well-constructed study with appropriate controls and analyses.

(2) Alternative interpretations of the data are systematically considered and eliminated via rational experiments. The authors are commended for a nice piece of experimental work.

(3) The vlPAG is a known region of pain modulation, and this study adds valuable insight to the circuit involved in fear-associated analgesia.

Weaknesses:

Only male mice are included in this study. [This has been explained and noted as a limitation.]

https://doi.org/10.7554/eLife.106826.2.sa3

Reviewer #2 (Public review):

Summary:

Wenke et al. investigated the role of vlPAG somatostatin-expressing neurons in the mediation of analgesia during defensive states. A newly developed paradigm of cued fear-conditioned analgesia, which consists of a combination of an auditory fear retrieval session and a pain test, was used to evaluate this cell population's contribution to fear-mediated analgesia. Optogenetic manipulation of vlPAG SST+ neurons modulated the responses to a nociceptive cue (Hot Plate) presented concomitantly with an aversively conditioned tone. At the same time, alterations in the freezing levels could be observed during optogenetic activation of vlPAG SST+ neurons. In order to disentangle the impact of these cells on analgesia from their impact on the expression of defensive behaviors, the authors performed electrophysiological recordings from the dorsal horn in the spinal cord of anesthetized mice. A vlPAG-RVM-DH pathway was identified to trigger nociceptive C-fibers upon optic activation of the RVM. Finally, pathway-specific activation of SST+ vlPAG-RVM neurons could abolish CS-induced analgesia.

Strengths:

The study addresses a relevant topic, that is, brainstem circuits for pain-modulatory mechanisms as part of defensive states evoked by threat. This is important because the circuit mechanisms underlying pain are still not fully understood, and defining molecular markers of cellular circuit substrates may support the identification of potential pharmaceutical

targets in treating pain. The authors confirm a previous study in that a somatostatin-positive cellular population presents a crucial vlPAG circuit element mediating anti-nociceptive effects. Key novelty aspects of the present study are the demonstration that these neurons seem to play a role specifically in threat-induced analgesia. This was possible by the elegant design and application of a novel fear analgesia paradigm, combined with cell- and pathway-specific optogenetics.

https://doi.org/10.7554/eLife.106826.2.sa2

Reviewer #3 (Public review):

Summary:

Conditioned analgesia refers to the ability of a learned fear cue to suppress pain-related behavior and neural activity. Understudied, the authors developed a novel conditioned analgesia procedure in which a cue that had been paired or unpaired with shock was played while a hot plate increased temperature. Compared to several control conditions, the authors found increased latency to a nociceptive response (paw licking). The authors identified somatostatin neurons in the periaqueductal gray as a likely mediator of the behavior. They then showed that: (1) stimulating vlPAG-SST neurons blocked nociceptive response latency increases to the CS+, (2) stimulating vlPAG-SST neurons suppressed fear retrieval freezing, (3) stimulating vs. inhibiting vlPAG-SST neurons drove opposing modulation of c-fibers and Aδ-fibers, (4) direct-projecting vlPAG SST neurons modulate freezing while RVM-projecting vlPAG SST neurons modulate conditioned analgesia.

Strengths:

These experiments have many strengths. The behavioral assay is chief among them. The assay is robust and controls for confounding factors to reveal a repeatable effect of a shock-paired cue to delay nociceptive responding. The optogenetic experiments provide the correct level of temporal precision, given the authors' time-specific interest in cued responding. Combining neuronal manipulations with spinal recordings is particularly innovative, especially in the context of more behavioral neuroscience-based assays. All-in-all, I found this to be an exceptionally strong set of experiments.

Weaknesses:

No obvious weaknesses were identified by this reviewer.

https://doi.org/10.7554/eLife.106826.2.sa1

Author response:

The following is the authors' response to the original reviews.

> ***Public Reviews:***
>
> ***Reviewer #1 (Public review):***
>
> *Summary:*
>
> *In the manuscript by Winke et al, the authors present evidence that fear-induced analgesia is mediated by somatostatin projection cells from the vlPAG to the RVM. This study uses a mouse model of fear-induced analgesia, and incorporates optogenetic circuit manipulation with behaviour and electrophysiology to gain a meaningful insight into a novel circuit involved in fear-induced analgesia.*

> *Strengths:*
>
> *(1) This is a well-constructed study with appropriate controls and analyses.*
>
> *(2) Alternative interpretations of the data are systematically considered and eliminated via rational experiments. The authors are commended for a nice piece of experimental work.*
>
> *(3) The vlPAG is a known region of pain modulation, and this study adds valuable insight to the circuit involved in fear-associated analgesia.*

We are very thankful to the referee for these positive comments.

> *Weaknesses:*
>
> *(1) Only male mice are included in this study.*

We thank the reviewer for this point. We used only males in this first study for practical reasons to work with a population as homogeneous as possible. However, taking sex differences in biological mechanisms into account, we included this restriction in the summary and discussion

> *(2) Animals are excluded from analyses based on clearly defined criteria, but it is not clear how many mice were excluded from each group.*

We thank the reviewers for raising this point. As stated in the Methods, we applied strict inclusion criteria for mice undergoing the hot-plate test, specifically a discrimination index ≥ 0.4 and a conditioning index ≥ 0.3. Using these criteria, 23% of wild-type mice were excluded for failing to meet the discrimination criterion. In the transgenic groups, an average of 20% of mice failed to meet the learning criteria, and an additional 12% were excluded due to incorrect opsin injection or misplaced optic fiber placement.

> *(3) The authors implement a pain sensitivity assay that involves a hot plate with progressively increasing temperature. The time to nociceptive responses is reported. Without reporting the actual temperature at which the mice respond, it makes it difficult to compare nociceptive responses to previously published work (which typically use a defined and static hotplate temperature).*

We thank the reviewer for this comment. We provided this information related to the actual temperature of the nociceptive response in the original manuscript in supplementary figures 1, 2 and 5.

> *(4) The authors present evidence that inhibition of SST vlPAG cells enhances spinal nociceptive electrophysiological responses, but the corresponding pain sensitivity is not altered (Figure 2, CS- condition). The reason for the discrepancy between electrophysiological and behavioural responses is not clear.*

We believe this comment arises from a misunderstanding of our results. In our study, inhibiting SST+ vlPAG cells did not increase nociceptive electrophysiological responses. Instead, it decreased spinal nociceptive transmission, as evidenced by reduced nociceptive field potentials and WDR responses in Figure 4c,e. Consistent with this electrophysiological effect, photoinhibition of SST+ vlPAG cells also produced behavioral analgesia, as evidenced by increased nociceptive response latency in the hotplate test under both CS− and CS+ conditions (Figure 2f). Therefore, our electrophysiological and behavioral findings are not contradictory but instead support the conclusion that inhibiting SST+ vlPAG cells reduces pain sensitivity regardless of defensive state. We will revise the text to clarify this point.

> ***Reviewer #2 (Public review):***
>
> *Summary:*
>
> *Wenke et al. investigated the role of vlPAG somatostatin-expressing neurons in the mediation of analgesia during defensive states. A newly developed paradigm of cued fear-conditioned analgesia, which consists of a combination of an auditory fear retrieval session and a pain test, was used to evaluate this cell population's contribution to fear-mediated analgesia. Optogenetic manipulation of vlPAG SST+ neurons modulated the responses to a nociceptive cue (Hot Plate) presented concomitantly with an aversively conditioned tone. At the same time, alterations in the freezing levels could be observed during optogenetic activation of vlPAG SST+ neurons. In order to disentangle the impact of these cells on analgesia from their impact on the expression of defensive behaviors, the authors performed electrophysiological recordings from the dorsal horn in the spinal cord of anesthetized mice. A vlPAG-RVM-DH pathway was identified to trigger nociceptive C-fibers upon optic activation of the RVM. Finally, pathway-specific activation of SST+ vlPAG-RVM neurons could abolish CS-induced analgesia.*
>
> *Strengths:*
>
> *The study addresses a relevant topic, that is, brainstem circuits for pain-modulatory mechanisms as part of defensive states evoked by threat. This is important because the circuit mechanisms underlying pain are still not fully understood, and defining molecular markers of cellular circuit substrates may support the identification of potential pharmaceutical targets in treating pain. The authors confirm a previous study in that a somatostatin-positive cellular population presents a crucial vlPAG circuit element mediating anti-nociceptive effects. Key novelty aspects of the present study are the demonstration that these neurons seem to play a role specifically in threat-induced analgesia. This was possible by the elegant design and application of a novel fear analgesia paradigm, combined with cell- and pathway specific optogenetics.*

We thank the referee for such positive feedback.

> *Weaknesses:*
>
> *Despite the convincing and rigorous experimental approach, the study leaves some interpretational room when it comes to the proposed circuit mechanism. This could either be addressed by additional experiments or by more discussion of alternative circuit layouts.*
>
> *Major Comments:*
>
> *(1) The paper by Zhang et al. (https://pubmed.ncbi.nlm.nih.gov/36641028/), which identified a role for vlPAG SOM+ neurons in mediating anti-nociception in neuropathic pain, needs to be referenced and its results discussed, if not reconciled. While functionally, both studies find an analgetic role of vlPAG SOM+ neurons projecting to the RVM, Zhang et al., using slice physiology, characterize those neurons as glutamatergic. In Figure 4E of Zhang et al. they find general (fear-independent) analgetic effects with PAG-RVM specificity by performing chemogenetic experiments.*

We thank the reviewer for highlighting this important point. We agree that the study by Zhang et al. is highly relevant and should be discussed in the revised manuscript. Their work shows that inhibiting vlPAG SST/SOM neurons with chemogenetic methods produces analgesia in a neuropathic pain model, and in our study, we similarly found that inhibiting SST+ vlPAG neurons increases hotplate response latency (Figure 2f), which aligns with an

analgesic effect. Additionally, we observed that activating SST+ vlPAG neurons suppresses fear-conditioned analgesia.

At the same time, there are important differences between the two studies that may explain the differences in interpretation. First, the behavioral paradigms are not identical. Zhang et al. used a hotplate protocol where animals were directly exposed to a nociceptive temperature, whereas in our study, we used a progressive temperature ramp and explicitly compared responses during a conditioned stimulus (CS+) and a non-conditioned control stimulus (CS−). These controls were important for us to distinguish fear-specific effects from more general effects related to stress, arousal, sensitization, or other non-associative processes.

Second, the two studies differ in experimental context. Zhang et al. examined this circuit in a neuropathic pain model, whereas our study focused on acute nociceptive processing and fear-conditioned modulation of pain. We therefore believe that the apparent discrepancy might reflect differences in pain state and behavioral context, rather than a direct contradiction.

Finally, Zhang et al. showed in slice recordings that SST+ vlPAG neurons provide excitatory input to RVM neurons. This is an important finding that we now address in the revised manuscript. At the same time, because the RVM contains heterogeneous neuronal populations with different projection targets and functions, these recordings alone do not prove that all recorded RVM neurons are part of the descending pathway controlling spinal nociception. Therefore, we have revised the Discussion to explicitly acknowledge Zhang et al. and to emphasize both the similarities and differences between the two studies.

> *It can be argued that in addition to the two functionally distinct inhibitory SOM subtypes hypothesized by Winke et al., there is another, excitatory subpopulation. Also, the different experimental conditions (chronic vs. acute pain, non-threat vs. fearful cues/contexts may recruit different vlPAG SOM+ populations. All of this is conceivable, yet I wonder whether the contrasting findings could more parsimoniously be reconciled. The author's own results presented here in Supplementary Figure 3 suggests that SOM+ vlPAG cells are colocalizing with glutamate and thus could also be excitatory. In addition to this rather complementary piece of evidence, a more extensive characterization of vlPAG neurons using IHC and slice physiology would be needed to justify the unambiguous identification of their inhibitory nature.*

We thank the reviewer for this thoughtful comment. We agree that our current data do not support a definitive conclusion that all SST+ vlPAG neurons are inhibitory. As the reviewer notes, our Supplementary Figure 3 shows that SST+ vlPAG cells can also co-localize with glutamatergic markers, which is consistent with the possibility of cellular heterogeneity within this population. We also agree that different experimental conditions, such as chronic versus acute pain and non-threatening versus fear-related contexts, may activate different SST+ vlPAG subpopulations.

Our intention was not to claim that SST+ vlPAG neurons constitute a uniform inhibitory population, but rather that SST+ cells are strongly represented among inhibitory neurons in the vlPAG. We agree, however, that more detailed characterization, including additional immunohistochemical analyses and slice physiology, is necessary to more definitively determine the neurotransmitter phenotype and functional connectivity of these neurons. We have therefore revised the text to temper our interpretation and to explicitly acknowledge the likely heterogeneity of SST+ vlPAG neurons, including the possibility of an excitatory subpopulation. We therefore modified the discussion accordingly:

“Our results align with the parallel inhibition- excitation model, where inhibitory and excitatory cells form two distinct, parallel descending pathways for pain modulation.

Indeed, previous research demonstrated the presence of an inhibitory pathway projecting throughout the PAG–RVM-spinal cord dorsal horn neuraxis. Our results complement this study by suggesting that one of these previously proposed parallel pathways is mediated by SST+ vlPAG cells and has a functional role in mediating analgesia. At the same time, our data indicate that vlPAG SST neurons are heterogeneous, with approximately one-third of these cells co-localizing with excitatory markers. Together with the recent observation that excitatory SST+ vlPAG neurons project to the RVM (Zhang et al., 2023), this raises the possibility that a subset of long-range SST+ vlPAG neurons contributes to an excitatory descending pathway within the PAG–RVM–spinal dorsal horn neuraxis. By contrast, local GABAergic SST+ vlPAG neurons may participate in local circuit mechanisms related to defensive-state expression, including freezing. Further anatomical and functional studies will be required to resolve these possibilities."

> *In the absence of a direct identification of these cells exclusively releasing GABA, an alternative explanation should be considered. What about looking at vlPAG SOM+ neurons as a putatively mixed bag of local, inhibitory interneurons and long-range, RVM-projecting excitatory cells? This model would then open up interesting questions as to the actual function of somatostatin as a modulator of vlPAG circuit activity and associated function, and from my perspective, would nicely fit into the view of PAG circuits as integrators of complex survival responses.*

We thank the reviewer for this insightful suggestion and agree that, in the absence of direct evidence that vlPAG SOM+/SST+ neurons are exclusively GABAergic, an alternative interpretation should be considered. In particular, we agree that this population may be heterogeneous and could include both local inhibitory interneurons and long-range excitatory neurons projecting to the RVM. We believe this is an important and constructive framework for interpreting our data, and we have revised the Discussion accordingly. In the revised text, we now explicitly acknowledge the likely heterogeneity of vlPAG SST+ neurons and discuss the possibility that distinct local and long-range SST+ subpopulations may contribute differently to defensive-state regulation and descending pain modulation. We agree with the reviewer on this point and have modified the discussion accordingly (see point above).

> *(2) "Our data indicate that the optogenetic inhibition of SST+ vlPAG cells promotes analgesia irrespective of the animal's defensive state. In contrast, the optogenetic activation of long-range SST+ vlPAG cells that project to the rostral ventromedial medulla (RVM) abolishes the analgesia mediated by fear behavior." (lines 32-35). Consider toning down these conclusions, as contrasting activation with inhibition of two different (though overlapping) populations cannot be fully conclusive. Alternatively, a pathway-specific (vlPAG-RVM) inhibitory experiment could help to fully understand the circuit mechanism and verify the necessity of these neurons.*

We thank the reviewer for raising this point. We agree that inhibition of the entire SST+ vlPAG population and activation of the long-range SST+ vlPAG neurons projecting to the RVM population are not directly equivalent manipulations. Our conclusion was intended at the level of observed functional effects: inhibition of SST+ vlPAG neurons promotes analgesia regardless of the defensive state, while activating long-range SST+ vlPAG neurons projecting to the RVM suppresses fear-conditioned analgesia. This occurs regardless of whether the SST vlPAG neurons are excitatory or inhibitory. To address the excitatory or inhibitory nature of SST vlPAG neurons, we have revised the discussion to include a reference to the Zhang et al study.

> *(3) Despite an overall very thorough reporting style, some information is missing from the manuscript:*

> *(a) In Figures 2d and f, what are the freezing levels during optogenetic manipulation? From Figure 3d, one can expect that freezing is inhibited during the hot plate test, which could bias the NC response towards shorter latencies.*

We thank the reviewer for this important comment. As shown in Figure 1e, we previously quantified freezing both at CS onset and at the time of the nociceptive response in the hot plate test. These analyses indicate that freezing levels at the time of the nociceptive response do not differ between the CS+ and CS− conditions. Therefore, the variation in hot plate response latency is unlikely to be due to differences in freezing at the time of response.

We acknowledge, however, that freezing was not directly measured during optogenetic manipulation in this experiment. Based on the temporal profile of freezing shown in Figure 1e, we still consider it unlikely that the effect of optogenetic manipulation on nociceptive latency is mainly caused by a change in freezing behavior.

> *(b) In Figure 5, the histological experiment showing the vlPAG-to-RVM pathway is presented by a qualitative image only. Here, some quantification would strengthen the finding.*

We thank the reviewer for this comment. The aim of the histological experiment in Figure 5 was to provide qualitative anatomical evidence that vlPAG projections reach the RVM and are positioned in close apposition to spinally projecting RVM neurons. We did not intend this experiment to serve as a quantitative characterization of connectivity. We agree that a more systematic quantification would be informative, but this would require additional dedicated experiments beyond the scope of the present manuscript.

> *(c) In Figures 6 c and d "Consistently, activation of the SST+ vlPAG-RVM pathway during CFCA had no impact on CS-presentation, whereas the same manipulation performed during CS+ blocked the increase in NC response latency compared to GFP controls." (line 194-196). Is it possible that the NC response cannot be any lower than the one during CS-, thus constituting a floor effect?*

We are thankful to the reviewer for this important point. We agree with the reviewer that this is indeed a possibility. We have added a sentence in the discussion to acknowledge this limitation.“Another possibility is that our nociceptive test with a slow ramp of temperature induces a floor effect on nociceptive response latency, which may limit the detection of further decreases in latency under certain conditions.”

> *(c) Connected to major point 1- this experiment is important for defining the circuit mode and therefore should be as convincing as possible. However, for the colocalization experiment in Supplementary Figure 3, the methodological description is missing and thus makes it hard to comprehend how this data set was generated (how many data points, etc.). The visual depiction of the results is non-standard and not easily graspable. Consider e.g., a Venn diagram.*

We apologize for this omission in the original manuscript. We have now provided this methodological information in the method section. We have now expanded the description of these data in the figure legend to ease the comprehension of the figure.

> ***Reviewer #3 (Public review):***
>
> *Summary:*
>
> *Conditioned analgesia refers to the ability of a learned fear cue to suppress pain-related behavior and neural activity. Understudied, the authors developed a novel conditioned analgesia procedure in which a cue that had been paired or unpaired with shock was played while a hot plate increased temperature. Compared to several control conditions,*

the authors found increased latency to a nociceptive response (paw licking). The authors identified somatostatin neurons in the periaqueductal gray as a likely mediator of the behavior. They then showed that: (1) stimulating vlPAG-SST neurons blocked nociceptive response latency increases to the CS+, (2) stimulating vlPAG-SST neurons suppressed fear retrieval freezing, (3) stimulating vs. inhibiting vlPAG-SST neurons drove opposing modulation of c-fibers and Aδfibers, (4) direct-projecting vlPAG SST neurons modulate freezing while RVM-projecting vlPAG SST neurons modulate conditioned analgesia.

Strengths:

These experiments have many strengths. The behavioral assay is chief among them. The assay is robust and controls for confounding factors to reveal a repeatable effect of a shock-paired cue to delay nociceptive responding. The optogenetic experiments provide the correct level of temporal precision, given the authors' time-specific interest in cued responding. Combining neuronal manipulations with spinal recordings is particularly innovative, especially in the context of more behavioral neuroscience-based assays. All-in-all, I found this to be an exceptionally strong set of experiments.

Weaknesses:

No obvious weaknesses were identified by this Reviewer.

Recommendations for the authors:

Comments from Reviewing Editor:

Summary

Three reviewers have assessed your manuscript on vlPAG somatostatin pathways contributing to conditioned analgesia. Conditioned analgesia refers to the ability of a learned fear cue to suppress pain-related behavior and neural activity. Understudied, the authors developed a novel conditioned analgesia procedure in which a cue that had been paired or unpaired with shock was played while a hot plate increased temperature. Compared to several control conditions, the authors found increased latency to a nociceptive response (paw licking). The authors identified somatostatin neurons in the periaqueductal gray as a likely mediator of the behavior. They then showed that: (1) stimulating vlPAG-SST neurons blocked nociceptive response latency increases to the CS+, (2) stimulating vlPAG-SST neurons suppressed fear retrieval freezing, (3) stimulating vs. inhibiting vlPAG-SST neurons drove opposing modulation of c-fibers and Aδ-fibers, (4) direct-projecting vlPAG SST neurons modulate freezing while RVM-projecting vlPAG SST neurons modulate conditioned analgesia.

Strengths

All three reviewers converged on multiple strengths. The assay developed was seen to be novel, rigorous, and included a variety of controls that convincingly demonstrated conditioned analgesia. Focusing on the ventrolateral periaqueductal gray, and more specifically on somatostatin-expressing cells, made prior sense, and the results more than justified this selection. Approaching the vlPAG and circuits with many converging methods provided further, compelling evidence for a role in conditioned analgesia.

Weaknesses

Specific weaknesses are described in the individual reviews. Generally, the following weaknesses were identified. The study only used male mice, a choice that should be better justified. Animals were reasonably excluded from analysis, but the final group ns for analyses were not always clear. Some statistical results lacked clarity. The relevance of these findings to prior work (particularly Zhang et al. 2023, Journal of Pain) was not

> *always described. Relatedly, the results would be better contextualized by appreciating and describing the likely diversity of somatostatin functional types and projection types.*
>
> *Recommendations*
>
> *(1) Provide rationale for only using male mice, discuss the limitation of the exclusion of females, and note that male mice were the subjects in the abstract.*

Thank you for this recommendation, we have mentioned this information in the abstract and in the discussion. We have also mentioned the limitations of not including female mice in the abstract and the discussion of the revised manuscript.

> *(2) Complete final report ns for each statistical analysis. If you have not already done so, please include full statistical reporting including exact p-values wherever possible alongside the summary statistics (test statistic and df) and, where appropriate, 95% confidence intervals. These should be reported for all key questions and not only when the p-value is less than 0.05 in the main manuscript.*

An extended table with all statistical tests and analysis for all figures has been provided in sup Table 1.

> *(3) Include example videos of CFCA sessions, demonstrating optogenetic effects.*

We understand the editor's request to include video material illustrating the behavioral responses. However, we would prefer not to include such videos in the manuscript, in accordance with our institution's guidelines and recommendations on the dissemination of animal experimentation footage. Importantly, all behavioral sessions were systematically video-recorded from both sides of the apparatus, allowing detailed offline analysis of the animals' responses. These recordings were carefully examined by an experienced experimenter to assess nociceptive behaviors, including jumping responses and licking of the stimulated hindpaw. This procedure ensured a reliable and accurate evaluation of pain-related behavioral reactivity. While the videos themselves cannot be included in the manuscript for the reasons mentioned above, we believe that the behavioral scoring procedures described in the Methods section provide a clear and rigorous description of how these responses were assessed. In addition, Figure 1 includes an example image illustrating hindpaw licking behaviour, which is typically more subtle and more difficult to identify than jumping responses. We therefore believe that this visual example, together with the detailed description of the scoring procedure and the quantitative data provided, adequately supports the interpretation of the behavioural results.

> *(4) Provide summary expression and ferrule placement figures.*

We thank the editor for this comment. We have now included schematic summaries of fiber placements for both SST and VIP mice used in this study, based on histological verification (Supplementary Figures 10 and 11). Representative images of viral expression are also provided (Figure 2a, Supplementary Figure 7b and f).

> *(5) Detail how behavior judgments were made.*

We thank the editor for emphasizing this important methodological point. During all behavioral sessions, mice were video-recorded simultaneously from both sides of the apparatus, allowing a comprehensive and unobstructed view of the animals' posture and movements throughout the experiment. These recordings were subsequently analyzed offline by an experienced experimenter trained to evaluate nociceptive behaviors. Pain-related behavioral responses were assessed based on well-established indicators of nociceptive reactivity. In particular, we quantified overt escape-like reactions such as jumping, which reflects a strong aversive response to the stimulus. In addition, we evaluated

more localized nociceptive behaviors directed toward the stimulated limb, including licking of the hindpaw. These measures are commonly used in rodent pain assays and provide reliable behavioral readouts of nociceptive sensitivity. The combination of bilateral video recordings and expert behavioral scoring ensured that both subtle and robust nociceptive responses could be accurately detected and categorized during the analysis.

> *(6) Provide the temperature at which nociceptive responses were initiated. Check grammar and references.*

The temperature at which nociceptive responses were initiated were originally reported in Supplementary Figure 1, 2 and 5.

> ***Reviewer #1 (Recommendations for the authors):***
>
> *(1) The authors use optogenetic manipulation of SST activity in the vlPAG to show that this cell type is involved in fear-induced analgesia. They include a valuable control to show that manipulation of another inhibitory cell type (VIP) also does not impact analgesia. It would be helpful to know the expression level of VIP cells in the vlPAG. Is this a predominant inhibitory projection cell in the vlPAG (besides SST)?*

We thank the reviewer for pointing this. While we did not quantify the expression level of VIP+ cells in the vlPAG in the present study, available data suggest that this population is relatively sparse compared to other inhibitory cell types. In particular, reference to the Allen brain atlas indicates that VIP gene expression in the vlPAG is limited and primarily localized around the fourth ventricle, within the lateral and ventrolateral PAG, rather than broadly distributed across the region. Consistent with this, we provide an example of viral expression in VIP-Cre mice in Supplementary Figure 7f, illustrating the restricted distribution of VIP+ neurons in the vlPAG. We have also provided a summary of ferrules placement for SST and VIP mice used in our study in Supplementary Figures 11 and 10, respectively.

> *(2) The numbers of animals dropped from each experiment should be indicated - perhaps on the statistics table?*

We thank the reviewer for pointing this.

As stated in the Methods, we applied strict inclusion criteria for mice undergoing the hot-plate test, specifically a discrimination index ≥ 0.4 and a conditioning index ≥ 0.3. Using these criteria, 23% of wild-type mice were excluded for failing to meet the discrimination criterion. In the transgenic groups, an average of 20% of mice failed to meet the learning criteria, and an additional 12% were excluded due to incorrect opsin injection or misplaced optic fiber placement.

> *(3) Line 105: "...,which activity..." change to "..., whose activity..."*

Done

> ***Reviewer #2 (Recommendations for the authors):***
>
> *(1) Please also provide absolute temperature values of the nociceptive response threshold.*

The temperature at which nociceptive responses were initiated was originally reported in Supplementary Figure 1, 2 and 5.

> *(2) It would be nice to see an example video of a CFCA session (with and without optogenetic manipulation).*

We understand the editor's and reviewer's request to include video material illustrating the behavioral responses. However, we would prefer not to include such videos in the

manuscript, in accordance with our institution's guidelines and recommendations on the dissemination of animal experimentation footage. Importantly, all behavioral sessions were systematically video-recorded from both sides of the apparatus, allowing detailed offline analysis of the animals' responses. These recordings were carefully examined by an experienced experimenter to assess nociceptive behaviors, including jumping responses and licking of the stimulated hindpaw. This procedure ensured a reliable and accurate evaluation of pain-related behavioral reactivity. While the videos themselves cannot be included in the manuscript for the reasons mentioned above, we believe that the behavioral scoring procedures described in the Methods section provide a clear and rigorous description of how these responses were assessed. In addition, Figure 1 includes an example image illustrating hindpaw licking behaviour, which is typically more subtle and more difficult to identify than jumping responses. We therefore believe that this visual example, together with the detailed description of the scoring procedure and the quantitative data provided, adequately supports the interpretation of the behavioural results.

> *(3) Please provide a schematic summary of fiber placements and opsin expressions confirmed by histological examinations.*

We thank the reviewer for this comment. We have now included schematic summaries of fiber placements for both SST and VIP mice used in this study, based on histological verification (Supplementary Figures 10 and 11). Representative images of viral expression are also provided (Figure 2a, Supplementary Figure 7b and f).

> *(4) "Valid nociception readout responses included jumping or licking the hindpaw." (Line 453). How was this evaluated- manually or automated, blinded etc.?*

We thank the reviewer for emphasizing this important methodological point. During all behavioral sessions, mice were video-recorded simultaneously from both sides of the apparatus, allowing a comprehensive and unobstructed view of the animals' posture and movements throughout the experiment. These recordings were subsequently analyzed offline by an experienced experimenter trained to evaluate nociceptive behaviors. Pain-related behavioral responses were assessed based on well-established indicators of nociceptive reactivity. In particular, we quantified overt escape-like reactions such as jumping, which reflects a strong aversive response to the stimulus. In addition, we evaluated more localized nocifensive behaviors directed toward the stimulated limb, including licking of the hindpaw. These measures are commonly used in rodent pain assays and provide reliable behavioral readouts of nociceptive sensitivity.The combination of bilateral video recordings and expert behavioral scoring ensured that both subtle and robust nociceptive responses could be accurately detected and categorized during the analysis.

> *(5) Line 226 REF33 doesn't seem to fit.*

The reference list has been updated. Related to this section in which we discuss the disinhibition mechanisms inducing nociception in chronic stress mice. We have cited the work of Samineni et al., 2015 (reference 15) and Tovote el al., (reference 23) both related to these disinhibition mechanisms.

Full sentence for reference 33 (now 35): "Two independent previous studies found that long-range inhibitory inputs from the central medial amygdala contact inhibitory cells within the vlPAG, implicated in different roles: the modulation of fear behavior (23) and nociceptive transmission (35)".

Ref 35 - Yin, W. et al. A Central Amygdala–Ventrolateral Periaqueductal Gray Matter Pathway for Pain in a Mouse Model of Depression-like Behavior. Anesthesiology 132,1175–119 (2020)

> *(6) Some minor language, semantic, and grammatical flaws.*

The manuscript has been evaluated for language, semantic and grammatical flaws

https://doi.org/10.7554/eLife.106826.2.sa0